Planetary Magnetic Fields and Fluid Dynamos

Chris A. Jones

Department of Applied Mathematics, University of Leeds, Leeds LS2 9JT, United Kingdom; email: cajones@maths.leeds.ac.uk

Annu. Rev. Fluid Mech. 2011. 43:583–614

First published online as a Review in Advance on September 22, 2010

The *Annual Review of Fluid Mechanics* is online at fluid.annualreviews.org

This article's doi: 10.1146/annurev-fluid-122109-160727

0066-4189/11/0115-0583$20.00

Keywords

geomagnetism, dynamo theory, dynamo simulations, planetary cores

Abstract

The magnetic fields of the planets, including the Earth, are generated by dynamo action in their fluid cores. Numerical models of this process have been developed that solve the fundamental magnetohydrodynamic equations driven by convection in a rotating spherical shell. New results from these theoretical models are compared with observations of the geomagnetic field and magnetic data gathered from space missions. The mechanism by which a magnetic field is created is examined. The effects of rotation and magnetic field on the convection are of paramount importance in the simulations. A wide range of simulations with different convection models, varying boundary conditions, and parameter values have been performed over the past 10 years. The effects of these differences are assessed. Numerical considerations mean that all dynamo simulations use much enhanced values of the diffusivities. We consider to what extent this affects results and show how the asymptotic behavior at low diffusion is starting to be inferred using scaling laws. The results of specific models relating to individual planets are reviewed.

1. INTRODUCTION

A series of space missions over the past 40 years has greatly enhanced our knowledge of the magnetic fields of the planets in our solar system, and also the magnetic fields of the larger satellites, which here we count as planets. We focus on the internal magnetic fields of the planets, so the active research topics of planetary magnetospheres and their interaction with the solar wind are not discussed here. The picture that has emerged is a remarkably complex one, with some planets having strong internal magnetic fields, and others having no discernible field in their core. There is evidence that Mars had a strong internal field in the past, but it does not have one at present.

It is generally believed that the internal magnetic fields are generated by dynamo action; that is, the field is created by fluid motion in planetary cores. Larmor (1919) suggested this possibility mainly in connection with the magnetic fields of sunspots, and Elsasser (1939) and Bullard (1949) gave the theoretical basis for the modern ideas of convection-driven dynamos. The temperature in planetary cores is well above the Curie temperature, so permanent magnetism cannot occur. In the absence of fluid motion, the Earth's magnetic field strength would decay by a factor *e* approximately every 15,000 years (see, e.g., Moffatt 1978), leaving a negligible field over the Earth's lifetime, 4.5 billion years. Many possibilities for generating planetary magnetic fields (e.g., the thermoelectric effect, magnetic monopoles) have been proposed, but all either have no reliable physical basis or have been shown to produce fields much smaller than those observed (Stevenson 2007).

Although Larmor's dynamo hypothesis has been generally accepted, the question of what is driving the fluid motion, and supplying the energy that is being lost to ohmic heating in planetary cores, is much more controversial. The most popular idea is that the dynamo is powered by thermal and compositional convection in the fluid core. In the case of the Earth, this means the fluid outer part of the core. Others have suggested that precession or tidal interactions might drive the dynamo (see, e.g., Malkus 1994, Tilgner 2007a), in which case the planet's rotation is the ultimate energy source for the magnetic field (see Tilgner 2007b for a review of the rotational dynamics of the Earth's core). In this review we concentrate on convection-driven dynamos, partly because their theory is much more developed than the theory of precession-driven dynamos, and partly because simple estimates suggest that convection can produce flows of the necessary order of magnitude, and the flows produced can be shown to give rise to dynamo action.

In parallel with the space exploration of planetary magnetism, considerable theoretical progress has been made in our understanding of convection-driven dynamos in spherical shells. This has been driven largely by the remarkable improvements in high-performance computers, which allow three-dimensional simulations in which the Navier-Stokes and induction equations are solved simultaneously. This only became feasible in the 1990s, but much progress has been made since then. Our understanding of planetary dynamos is more advanced than our understanding of stellar dynamos, because the magnetic Reynolds number, *Rm*, in planets is generally moderate, and the induction equation is therefore numerically tractable. There are serious theoretical difficulties with nonlinear dynamos in the high *Rm* limit, which emerged in the 1990s and which have not yet been fully resolved (see, e.g., Hughes 2007). There are nevertheless problems with current planetary dynamo simulations (see, e.g., Jones 2000), because two small parameters, the Ekman number and the magnetic Prandtl number, appear in the fundamental equations. Dynamo simulations cannot reach the very small values of these parameters that are found in planetary cores, and so we still need to understand the limiting behavior of the models as these parameters become small, which remains a challenging problem. There have been some important theoretical advances in our understanding of convection in the presence of rotation and magnetic field that have helped the interpretation of the results emerging from the very complex simulations. There are also a number of laboratory dynamo and magnetohydrodynamic experiments, which also cannot reach the planetary regime, but nevertheless do probe a different part of the parameter space, which helps to build up understanding.

The planets are conveniently divided into three groups (Stevenson 2003): the terrestrial planets with rocky interiors, some of which have fluid cores; the gas giants Jupiter and Saturn, whose composition is primarily hydrogen and helium; and the ice giants, Uranus and Neptune, which have deep gaseous atmospheres but also have more heavy elements than in solar composition. Far more is known about the Earth than the other planets, because the observation history is longer and more accurate, and seismology gives us detailed information about the nature of the core. Three terrestrial planets have magnetic fields strong enough to suggest an internal field and therefore a dynamo: the Earth, Mercury, and Ganymede, the largest moon of Jupiter. The strong remanent magnetism of Mars, discovered by the Global Surveyor mission (Acuña et al. 1999), suggests that Mars once had a dynamo but that it ceased to operate probably about 350 million years after the planet's birth. Venus has no measurable internal field. Our Moon has patches of crustal magnetization, which may be remnants of an era when the Moon had a working dynamo, but it is also possible that lunar magnetic fields were created during meteorite impacts (Stevenson 2003). None of the other larger satellites in the solar system have strong internal fields, although there are induction effects in the inner Jovian satellites due to their motion through Jupiter's magnetic field.

Previous review articles relating to this material are Busse (2000), which discusses the then existing laboratory experiments and spherical convection-driven dynamo models; Kono & Roberts (2002), which covers the geomagnetic field and its relation to dynamo simulations; and Jones (2003, 2007a), which review magnetic fields in planets. Christensen & Wicht (2007) focused on numerical dynamo simulations, and Jones (2007b) addressed thermal and compositional convection in the core.

2. THE GEOMAGNETIC FIELD

Magnetic fields generated internally can be represented in the electrically insulating region above the core by the spherical harmonic expansion for the potential

$$\Psi = r_s \sum_{n=1}^{\infty} \sum_{m=0}^{m=n} \left(\frac{r_s}{r}\right)^{n+1} P_n^m(\cos\theta)(g_n^m \cos m\phi + h_n^m \sin m\phi), \tag{1}$$

where the magnetic field $\mathbf{B} = -\nabla\Psi$, and r, θ, and ϕ are spherical polar coordinates, with θ as the colatitude. Here the associated Legendre polynomials have the partial Schmidt normalization (see, e.g., Merrill et al. 1996, p. 28), and the coefficients g_n^m and h_n^m are the Gauss coefficients. Planetary magnetic fields, including that of the Earth, are usually specified by their Gauss coefficients. Equation 1 can be used to reconstruct the field either at the planetary surface $r = r_s$ or at the core-mantle boundary (CMB), $r = r_{cmb} = 3.48 \times 10^6$ m for the Earth.

2.1. The Magnetic Field Spectrum

Figure 1*a* shows the radial component of the Earth's field at the surface. Note that the axial dipole g_1^0 component dominates the picture. **Figure 1*b*** shows the field at the CMB. It is still essentially dipolar, but the field clearly has much more small-scale structure, as well as being about 10 times stronger. Also of interest in **Figure 1*b*** is the large reversed field patch in the South Atlantic. This feature has been growing over the past few 100 years, which is the main reason why the dipole

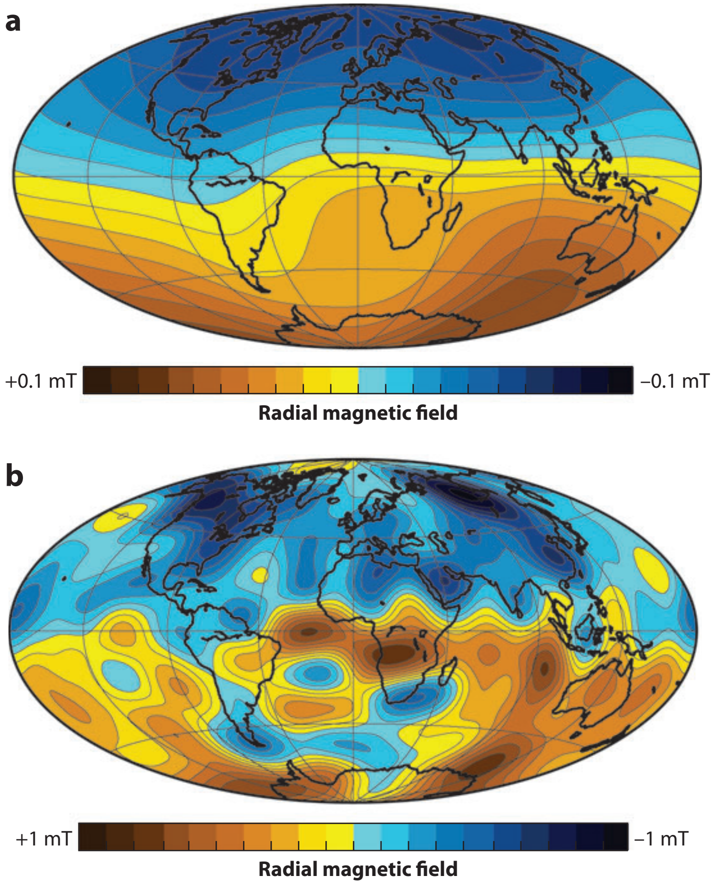

Figure 1

(*a*) The radial component of the Earth's magnetic field at the surface and (*b*) at the core-mantle boundary, both using the Hammer-Aitoff projection. In panel *b*, shorter wavelengths may be present in the true field, but they have to be filtered out because of crustal-field contamination. Figure provided by R. Holme.

component of the geomagnetic field is in decline (Gubbins et al. 2006). The relative content of higher harmonics is measured by the Lowes-Mauersberger spectrum

$$R_n = \left(\frac{r_s}{r}\right)^{2n+4} (n+1) \sum_{m=0}^{n} [(g_n^m)^2 + (h_n^m)^2], \tag{2}$$

which is fairly constant with n up to degree about 12 if r is evaluated at the CMB (see, e.g., Maus et al. 2005). For higher n, the geomagnetic core field is obscured by crustal magnetism. The spectrum must tail off at some value of $n > 12$ because otherwise the ohmic dissipation would be too large. A recent discussion of bounds on the ohmic heat dissipation for the geomagnetic field is given by Jackson & Livermore (2009). Another interesting feature of **Figure 1*b*** is the string of flux patches just south of the equator from the mid-Atlantic, which are propagating westward (Jackson 2003). The time dependence, called the secular variation, is measured by continuous monitoring of the field by satellites and magnetic observatories.

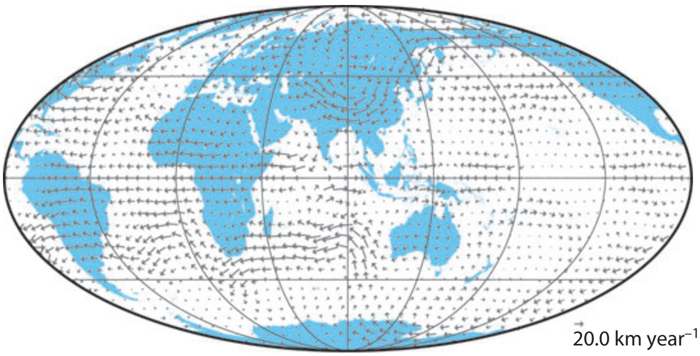

Figure 2

Core flow inferred from secular variation observations using the tangential geostrophy assumption. Figure reproduced with permission from Holme & Olsen (2006).

2.2. The Core Flow

The secular variation enables the velocity below the CMB to be reconstructed, provided some assumptions are accepted. The most common assumption is the frozen flux hypothesis (Roberts & Scott 1965),

$$\frac{\partial B_r}{\partial t} = -\nabla_H \cdot (\mathbf{u}_H B_r), \tag{3}$$

where ∇_H is the horizontal gradient, $\mathbf{u}_H$ is the tangential flow just below the CMB, and B_r is the radial component of the magnetic field. As this is only one equation for two unknown velocity components, an additional constraint from the equation of motion is required. A common assumption is tangential geostrophy, which is $\nabla_H \cdot \cos\theta \mathbf{u}_H = 0$, although several others have been used (Holme 2007). **Figure 2** shows the tangential components of $\mathbf{u}$ that result from these assumptions (Holme & Olsen 2006). The most important deduction for dynamo theory is the estimate of the typical core velocity, which is consistent with that expected from thermal and compositional convection in the core and is also capable of generating magnetic field by dynamo induction (see below).

2.3. Reversals and Excursions

The geomagnetic field reverses polarity rather randomly. The reversal rate is typically once every 0.3 Myr (see Merrill et al. 1996 for a full discussion), but reversals are completed relatively quickly, on a timescale of around 20,000 years only. There have been long periods, around 40 Myr, during which the field has not reversed at all, the most famous being the Cretaceous superchron, 83–124 Myr before present. A rather controversial observation is that the dipole axis of the field has preferred longitude paths during reversal (Hoffman 1992), discussed by Glatzmaier & Coe (2007). In addition to the full reversals, the dipole axis has much more frequent excursions (e.g., Valet et al. 2005), which may be thought of as failed reversals because the field strength drops and the dipolar component moves away from the geographical polar axis, but eventually the field recovers its original polarity.

3. DYNAMO MODELS

Dynamo simulations in spherical geometry have mostly used the Boussinesq approximation, although recently anelastic dynamo models have been developed. These have mostly been used

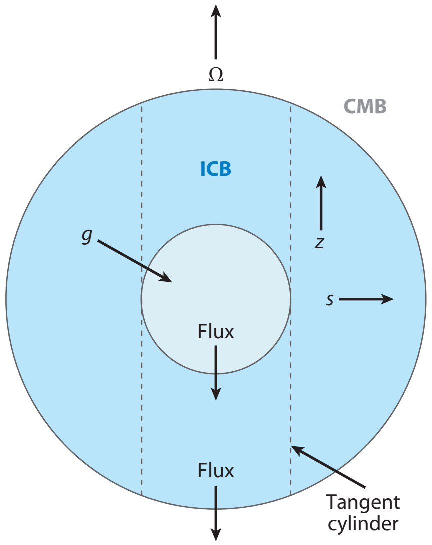

Figure 3

Geometry used for spherical shell geodynamo simulations. The fluid outer core lies between the inner-core boundary (ICB) and core-mantle boundary (CMB). Gravity is directed radially inward, and the heat flux is carried outward.

to investigate stellar dynamos, with the ASH (anelastic spherical harmonic) code (Clune et al. 1999) perhaps the best-known code. Some work has been done on compressible models for the giant planets (Jones & Kuzanyan 2009), and more is in progress. The configuration used by the Boussinesq codes is shown in **Figure 3**. The fluid outer core lies between the inner-core boundary (ICB) and the CMB. The inner core is an electrically conducting solid, mostly iron. Spherical polar coordinates r, θ, and ϕ are used in the computations, but cylindrical coordinates s, ϕ, and z are also useful to discuss results. There is rotation Ω about the z axis, and gravity is radially inward, and of magnitude proportional to r, appropriate for a uniform sphere. Centrifugal acceleration is neglected. The unit of length is the gap width $d = r_{cmb} - r_{icb}$, and for the Earth $r_{icb} = 1.22 \times 10^6$ m and $d = 2.26 \times 10^6$ m. The tangent cylinder, marked in **Figure 3**, is an imaginary cylinder, but it does divide the core into regions where the dynamical behavior is rather different.

We use the magnetic diffusion time d^2/η as the unit of time, where η is the magnetic diffusivity, estimated at 2 $m^2\,s^{-1}$ in metallic cores. The unit of velocity is then η/d, so the dimensionless velocity is a direct measure of the magnetic Reynolds number $Rm = U_* d/\eta$, where U_* is the typical core velocity. The unit of magnetic field is $(\Omega\rho\mu\eta)^{1/2}$, where ρ is the density ($\sim 10^4$ kg m^{-3}), and $\mu = 4\pi \times 10^{-7}$ in SI units is the permeability of free space, so a magnetic field of strength 1 has an Elsasser number $\Lambda = B_0^2/\Omega\rho\mu\eta$ of unity. In the Earth's core this unit is about 1.4 mT or 14 Gauss.

The dimensional Boussinesq equation of motion is

$$\rho \frac{D\mathbf{u}}{Dt} + 2\rho\mathbf{\Omega} \times \mathbf{u} = -\nabla p + \mathbf{j} \times \mathbf{B} + \rho\nu\nabla^2\mathbf{u} + \frac{\rho g_0}{r_{cmb}}(\alpha T + \xi)\mathbf{r}. \tag{4}$$

Here $\mathbf{u}$ is the velocity, p is the pressure, ν is the kinematic viscosity, and $\mathbf{j}$ is the current density, which is $\nabla \times \mathbf{B}/\mu$ by Ampère's law. g_0 is gravity at the CMB, and the buoyancy term has a thermal part αT, where α is the coefficient of thermal expansion, and a compositional component ξ, where ξ is the mass fraction of light material (believed to be sulphur and oxygen in the Earth's core).

The dimensionless form is

$$\frac{E}{Pm}\frac{D\mathbf{u}}{Dt} + 2\hat{\mathbf{z}} \times \mathbf{u} = -\nabla p + (\nabla \times \mathbf{B}) \times \mathbf{B} + E\nabla^2\mathbf{u} + \frac{Ra\,E\,Pm}{Pr}(T + \xi)\frac{\mathbf{r}}{r_{cmb}}. \quad (5)$$

Here the unit of temperature is ΔT, the superadiabatic temperature difference across the core, and the unit of ξ is $\alpha\Delta T$.

The dimensionless induction equation is

$$\frac{\partial \mathbf{B}}{\partial t} = \nabla^2\mathbf{B} + \nabla \times (\mathbf{u} \times \mathbf{B}), \quad (6)$$

and the temperature and composition equations are

$$\frac{\partial T}{\partial t} = \frac{Pm}{Pr}\nabla^2 T - \mathbf{u} \cdot \nabla T + Q, \quad (7)$$

and

$$\frac{\partial \xi}{\partial t} = \frac{Pm}{Pc}\nabla^2 \xi - \mathbf{u} \cdot \nabla \xi + Q_\xi, \quad (8)$$

and we also have

$$\nabla \cdot \mathbf{B} = \nabla \cdot \mathbf{u} = 0 \quad (9)$$

for Boussinesq fluid.

The dimensionless parameters are

$$Ra = \frac{g_0 \alpha \Delta T\, d^3}{\nu\kappa}, \quad Pr = \frac{\nu}{\kappa}, \quad Pm = \frac{\nu}{\eta}, \quad Pc = \frac{\nu}{\kappa_\xi}, \quad E = \frac{\nu}{\Omega d^2}, \quad (10)$$

where *Ra* is the Rayleigh number, *Pr* the Prandtl number, *Pm* the magnetic Prandtl number, *Pc* the compositional Prandtl number, and *E* the Ekman number. κ and κ_ξ are the thermal and compositional diffusivities, respectively. The terms Q and Q_ξ represent internal heating (or cooling) and internal compositional sources. To complete the model we must specify the radius ratio r_{icb}/r_{cmb}, taken as 0.35 for the Earth's core, and the boundary conditions. The usual estimate for the molecular value of E is 10^{-15}, way below what can be achieved numerically. Even if we suppose a turbulent diffusion increasing the viscosity to the value of the magnetic diffusivity, and there is no compelling physical reason to assume so large a turbulent diffusion, we still have $E \sim 5 \times 10^{-9}$, also below anything numerically possible. The fluid Prandtl number in metallic cores is typically 0.1, and the compositional Prandtl number is large, but the magnetic Prandtl number is very small, of order 10^{-6}. This is far below what can be achieved in simulations. It is often argued that turbulence will enhance the effective values of the Prandtl numbers toward unity. This may well be the case, but our current understanding of the nature of core turbulence is very limited. The possible form of small-scale turbulence to be expected in the core and its effects are discussed by Braginsky & Meytlis (1990) and Braginsky & Roberts (1995). The very slow flows, the rapid rotation, and strong influence of the magnetic field mean that we are far from regimes that can be studied experimentally or numerically.

To estimate the Rayleigh number inside the core, we need to know the superadiabatic temperature difference between the ICB and CMB. This is very much less than the actual temperature difference, which is of order 10^3 K, because the core is almost certainly very close to adiabatic stratification. In Section 6 below, we estimate the typical temperature fluctuation as having an order of magnitude of 10^{-3} K. In practice, the Rayleigh number is often chosen so that a sensible value of the magnetic Reynolds number is found.

Equations 5–10 form a complete set of equations, which together with appropriate boundary conditions can be integrated forward in time. Another issue is the choice of heat and composition sources, Q and Q_ξ. As the inner core grows, the light-element composition increases, and this is an effective uniform sink. Similarly, a gradual cooling of the core is an effective heat source. As more heat is conducted down the adiabat near the CMB than near the ICB, heat flux is removed from the convection to appear as conduction, so this is an effective heat sink. These rather complicated heat and composition source issues are discussed in detail in Anufriev et al. (2005).

In practice, not much attention has been paid to the case with both compositional and thermal driving. If the Prandtl numbers are close to unity (as may be the case if turbulent diffusion dominates), and similar boundary conditions are used for temperature and composition, temperature and composition may be combined into one codensity variable (Braginsky & Roberts 1995). Partly because of this, and for reasons of simplicity, most dynamo models have used only one buoyancy source, usually called temperature.

To interpret the solutions that emerge from integration of these equations, the linear theory of rapidly rotating convection in spherical shells is essential. This linear theory is now fairly well understood. Roberts (1968) and Busse (1970) established that convection onsets in tall thin columns. Numerical solutions showing the columns spiralling outward in the s-ϕ plane were found by Zhang (1992), and the full small E asymptotic theory was evaluated by Jones et al. (2000) and Dormy et al. (2004). There is now excellent agreement between numerics and asymptotics, and the theory has recently been extended to anelastic compressible convection by Jones et al. (2009).

The first time-dependent numerical solutions of the full magnetohydrodynamic equations given in Equations 5–10 in spherical geometry appeared in the mid-1990s (Glatzmaier & Roberts 1995, 1996a,b, 1997; Jones et al. 1995; Kageyama et al. 1995; Kuang & Bloxham 1997). It soon became apparent that steady dipolar dynamos, and dynamos that occasionally reversed, were possible. The flow speeds generating the fields give magnetic Reynolds numbers similar to those indicated by the core flow measurement techniques of Section 2.2.

Many different boundary conditions have been used, and the effects of different boundary conditions are reviewed in Section 5 below. The most commonly studied, for reasons of simplicity rather than their relevance to planetary models, are no-slip boundary conditions, tangential $\mathbf{u}$ vanishing on both boundaries, constant-temperature boundaries, and a magnetic insulator in both inner core and mantle. The standard model also has no heat sources, but is driven by a uniform heat flux entering through the ICB and leaving through the CMB. All these assumptions can be criticized, but they do form a useful basis from which to explore the effects of making different assumptions. The dynamo benchmark (Christensen et al. 2001) was a standard model case with $Ra = 10^5$, $E = 10^{-3}$, $Pr = 1$, and $Pm = 5$, which was used by a number of different codes to establish their accuracy. The solution is steady in a drifting frame provided that a suitable initial value is used for the magnetic field. This steadiness in a drifting frame is an unusual property for convection-driven dynamos. The norm is that the flow has gone through several bifurcations as Ra is increased and has chaotic time dependence before the magnetic field starts to grow. A more typical case for the standard model is at $Ra = 7.5 \times 10^6$, $E = 10^{-4}$, $Pr = Pm = 1$, computed by Christensen et al. (1999) and confirmed by Sreenivasan & Jones (2006a). A snapshot of the radial component of the magnetic field and the radial velocity at $r = r_{icb} + 0.8d$ is shown in **Figures 4*a*,*b***. Notable features are the strong dipolar dominance of the field (more dipolar than the Earth at the CMB; see **Figure 1*a***), the strong flux patches where the tangent cylinder meets the CMB, and the slightly weaker field at the poles (similar behavior in the geomagnetic field). The radial velocity plot shows that the convection occurs in columnar structures, with a long length scale parallel to the rotation axis and a comparatively short length scale transverse to z, tall thin columns. Movies of the radial field show that it drifts westward, as does the velocity field pattern in **Figure 4*b***. The field and flow are not steady in a drifting frame; individual flux patches and convection columns continually grow and decay. The ϕ average of the azimuthal field, B_ϕ, is shown in **Figure 4*c***.

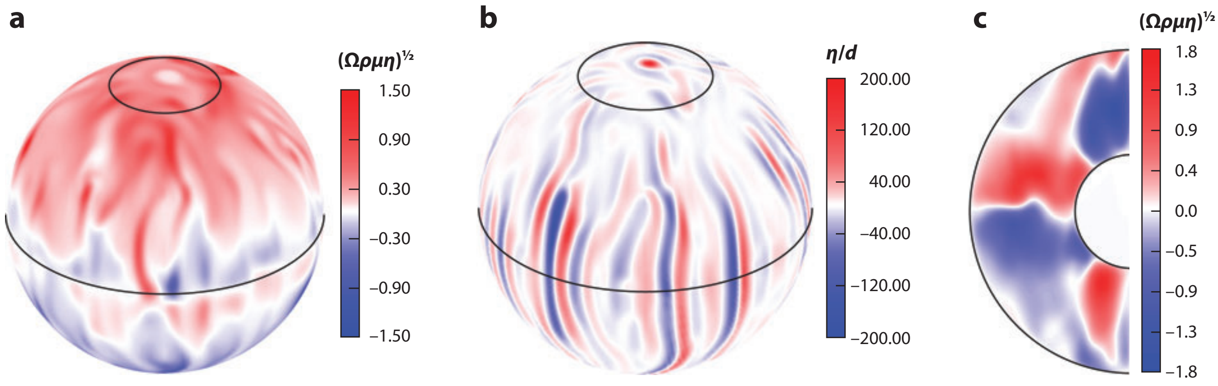

Figure 4

Snapshot of a dynamo simulation: $Ra = 7.5 \times 10^6$, $E = 10^{-4}$, and $Pr = Pm = 1$: (*a*) The radial component of the magnetic field B_r at the core-mantle boundary, (*b*) radial velocity u_r at $r = r_{ICB} + 0.8d$, and (*c*) a meridional section of the azimuthally averaged azimuthal field B_ϕ.

Note that it is mainly antisymmetric about the equator, which is consistent with the meridional field being mainly dipolar. The magnetic structures that are generated inside the core have been visualized by Aubert et al. (2008b).

4. THE DYNAMO MECHANISM

In this section we focus on the dynamo mechanism generating the magnetic fields in the dipolar cases such as that shown in **Figure 4**. In these cases, the magnetic field is created in the convection columns, and the mechanism is essentially that for α^2 dynamos (see, e.g., Moffatt 1978). Our description of the dynamo process follows Olson et al. (1999). **Figure 5** shows an illustration of the flow in four convective columns. The columns are drawn as circular, but in reality each column may have a more complicated cross section. The primary flow is the rotation of each column about its z axis, with alternate columns being cyclonic (anticlockwise viewed from the north, adding to the vorticity of the rotating planet) or anticyclonic (clockwise viewed from the north, reducing the planetary vorticity). This flow is driven by the convection near the equatorial region, with hot rising fluid carried out from the ICB in the positive s direction toward the CMB. Similarly, cold fluid falls back between the columns. This columnar flow on its own cannot drive a dynamo. Indeed no purely two-dimensional flow can drive a dynamo (Zeldovich 1957). The secondary flow up and down the columns is therefore crucial. The direction of the secondary flow is such that it diverges in the z direction at the equator in the anticyclones and converges at the equator in the cyclones. As the fluid is incompressible, this means that flow must converge in the ϕ and s directions in the anticyclones near the equator. This convergence leads to an accumulation of B_z in the anticyclones near the equator (Kageyama & Sato 1997). Similarly, a meridional field (that is, in the r and θ directions) accumulates in cyclones near the CMB.

Figure 6 illustrates the process by which magnetic field in the ϕ direction is converted into a meridional field. The symmetry of the initial B_ϕ field can be seen in **Figure 4*c***. In **Figure 6*a***, which is taken to be in the northern hemisphere, the secondary flow stretches out B_ϕ, creating B_z. This generates B_z locally, but there is no nonzero average over ϕ. However, as shown in **Figure 6*b***, the primary flow sweeps the positive B_z field toward the ICB and the negative B_z toward the CMB, creating a nonzero average in ϕ. In the southern hemisphere, B_ϕ has the opposite

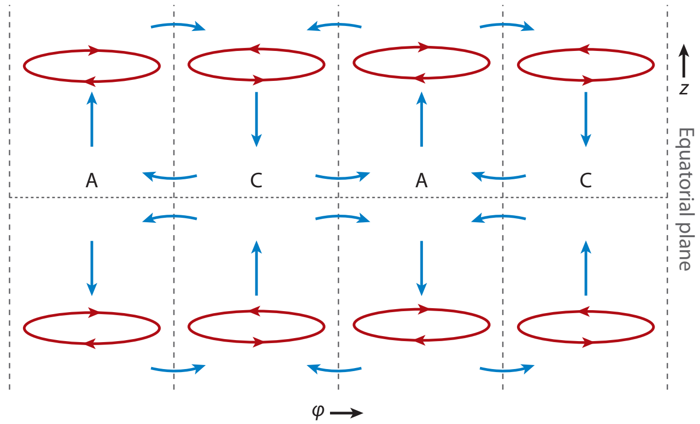

Figure 5

Illustration of the flow in the convective columns. The primary (*red*) flow shows the cyclonic (C) and anticyclonic (A) rotation of the convecting columns. The secondary (*blue*) flow shows the flow up and down the columns and its recirculation near the equator and the core-mantle boundary.

sign, and the secondary flow also has the opposite sign, so the created B_z has the same sign. The meridional field created therefore has a dipolar nature, with B_z positive near the ICB, in agreement with **Figure 4*a***. The negative B_z generated in this process is mostly pushed out of the core altogether, which is allowed by the insulating boundary conditions. This mechanism relies (implicitly) on the relatively low magnetic Reynolds number on the roll length scale. If we denote the typical thin length scale across a roll by $L_\perp$, the local $Rm = U_* L_\perp/\eta \ll U_* d/\eta$ is sufficiently small so that the field is not advected though more than a moderate angle before diffusion kicks in, thus ensuring that all the generated B_z has the appropriate sign. In mathematical terms, we are in the first-order smoothing regime of Moffatt (1978). For simplicity, we concentrate here on B_z production, but similar arguments apply to B_s production, except that now it is the primary flow

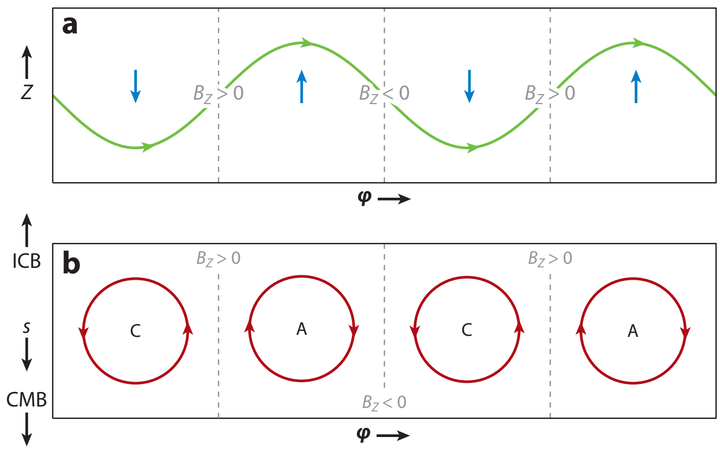

Figure 6

Illustration of the creation of B_z from B_ϕ in the northern hemisphere. (*a*) A B_ϕ magnetic field line (*green*) is stretched by the secondary flow of **Figure 5**. (*b*) The created B_z field is separated by the primary flow, so that positive B_z moves to the inner-core boundary (ICB), and negative B_z moves to the core-mantle boundary (CMB).

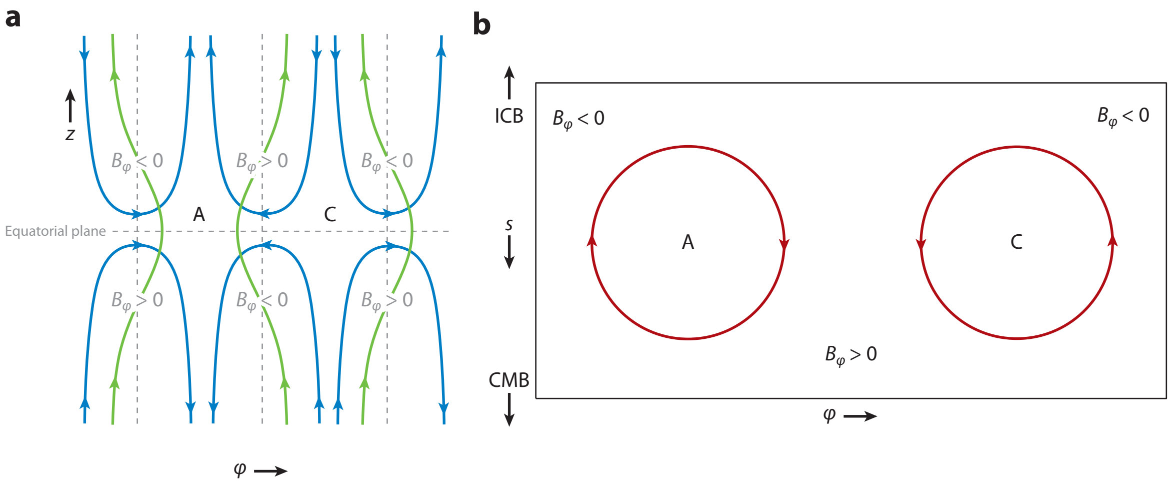

Figure 7

Illustration of the creation of B_ϕ from B_z in the northern hemisphere. (*a*) A B_z magnetic field line (*green*) is stretched by the secondary flow of **Figure 5**. (*b*) The created B_ϕ field is separated by the primary flow, so that negative B_ϕ moves to the inner-core boundary (ICB), and positive B_ϕ moves to the core-mantle boundary (CMB).

that generates B_s and the secondary flow that separates out the positive and negative B_s. In the northern hemisphere, positive B_s is moved toward the pole and negative B_s toward the equator, with the opposite taking place in the southern hemisphere, consistent with the dipolar nature of the field.

The creation of negative and positive B_s from B_ϕ across individual rolls just above and below the equator gives rise to reversed flux patches, which are visible in **Figure 4*a***. The u_z flow will push these reversed flux patches together, and they will be destroyed by diffusion across the equator. However, the u_z flow is weak near the equator, and so the near-equatorial reversed flux patches appear in many simulations. Interestingly, the present geomagnetic field does not show this behavior; the reversed field patches in the Earth's CMB seem to occur mainly at high latitudes. This is perhaps the main difference between the fields generated by the simulations in the dipolar regime at moderate Rayleigh number and the actual geomagnetic field.

Figure 7 illustrates the process by which the B_z field is converted back to an azimuthal field. In the solar dynamo, the azimuthal field comes from a differential rotation stretching out the meridional field, the ω-effect. It was therefore quite a surprise when convection-driven dynamo models were shown to be generating an azimuthal field not by the ω-effect but through the α-effect also, hence the name α^2 models. This is possibly because the magnetic field itself tends to strongly reduce the shear driven by Reynolds stresses (see, e.g., Aubert 2005), whereas in the solar dynamo the field only weakly affects the differential rotation. In **Figure 7*a***, an initial field line in the z direction is stretched into the ϕ direction by the secondary flow (see **Figure 5**). **Figure 7*b***, the situation in the northern hemisphere, shows that the positive B_ϕ created is swept toward the CMB, whereas negative B_ϕ is swept toward the ICB. Now with insulating boundaries at the ICB, B_ϕ vanishes at the ICB, so the negative B_ϕ is lost by diffusion. Therefore, net positive B_ϕ is created, in agreement with **Figure 4*c***.

We can view these mechanisms in terms of the mean ϕ-averaged field $\overline{\mathbf{B}}$ and the small-scale fluctuating parts $\mathbf{b}'$ produced by the convection rolls, which are highly nonaxisymmetric. Ohm's law can then be written

$$\eta \nabla \times \overline{\mathbf{B}} = \eta \mu \bar{\mathbf{j}} = \overline{\mathbf{E}} + \overline{\mathbf{U}} \times \overline{\mathbf{B}} + \overline{\mathbf{u}' \times \mathbf{b}'}, \tag{11}$$

and we are interested in the mean current produced by the mean of the fluctuating convective terms. The dipolar field with B_z positive near the ICB and negative outside is produced by a positive azimuthal current, so we need the ϕ component of $\overline{\mathbf{u}' \times \mathbf{b}'}$, $\overline{u'_z b'_s - u'_s b'_z}$, to be positive. **Figure 6** focuses on the term $\overline{u'_s b'_z}$. The induction equation for the fluctuating term (ignoring any mean flow $\overline{\mathbf{U}}$) is

$$\frac{\partial \mathbf{b}'}{\partial t} = \overline{\mathbf{B}} \cdot \nabla \mathbf{u}' + \eta \nabla^2 \mathbf{b}', \tag{12}$$

assuming that derivatives of the mean quantities are small compared with derivatives over the short fluctuating length scales. Taking the z component and using the azimuthal $\overline{B}_\phi$, we get the rate of growth of b'_z as $\overline{B}_\phi/s\ \partial u'_z/\partial\phi$. We assume this field builds up for a time Δt and then comes into balance with diffusion, so $b'_z \sim \Delta t \overline{B_\phi}/s\ \partial u'_z/\partial\phi$. Note this argument is only valid provided diffusion is strong enough for equilibrium to be achieved before fluctuating fields can build up sufficiently to change the B_ϕ significantly; this is where the first-order smoothing assumption (Moffatt 1978) enters the argument. Note also that this result for b'_z is in accord with the illustrated argument in **Figure 6*a***. **Figure 6*b*** shows that $u'_s b'_z$ is negative, so this part of the fluctuating term does indeed generate a positive $\overline{j_\phi}$ current as required to maintain the dipole. Considering **Figures 6** and **7**, it is not difficult to see that the term $u'_z b'_s$ will be positive, and so this term reinforces the creation of positive j_ϕ. This argument gives $\overline{j_\phi} = \Delta t \overline{B_\phi}/s\ [u'_z \partial u'_s/\partial\phi - u'_s \partial u'_z/\partial\phi]$, and the terms in square brackets are the dominant terms of $\mathbf{u}' \cdot \nabla \times \mathbf{u}'$, the kinetic helicity, because the convection varies most rapidly in the ϕ direction. It is this nonzero helicity, mainly antisymmetric about the equator, that gives rise to the dynamo action seen in these dipolar models. The secondary flow of **Figure 5** is therefore an essential part of the dynamo. Similar arguments can be used to understand the creation of $\overline{B_\phi}$ from the meridional field. **Figure 7** focuses on the z component of the current in Equation 11, and the term $u'_s b'_z$, which has positive mean, but similar arguments apply to the other terms giving rise to meridional current.

5. EXPLORING THE PARAMETER SPACE

The Boussinesq dynamo equations given in Equations 5–10 have been used for a very large number of simulations. However, many different choices have been made for the parameters, the boundary conditions, and the form of the internal heating, with the consequence that it can be quite difficult to relate the results from different authors, and it can seem as though by an appropriate choice almost any result can be obtained. There are, however, some recurrent features that can serve as a guide through this wilderness. We start by considering the effect of varying the parameters in the standard model, that is, when there is no internal heating and the temperature is fixed at the boundaries, which are no slip and electrically insulating.

5.1. The Standard Model

The case of the standard model has been explored by Olson et al. (1999), Christensen et al. (1999), Kutzner & Christensen (2002), and Sreenivasan & Jones (2006a), among others. There are five dimensionless parameters that describe this model: the radius ratio, Ra, E, Pm, and Pr. Sometimes $q = Pm/Pr$ is used in place of Pm. We describe here only radius ratio $= 0.35$, the Earth-like value, leaving different radius ratios to Section 7. If we set $Pr = 1$, dynamos obtained as the three remaining parameters are varied are illustrated in **Figure 8**. At moderate $E = 10^{-3}$, fairly high Pm is needed to obtain any dynamo, a result noted as early as 1989 by Zhang & Busse, which caused

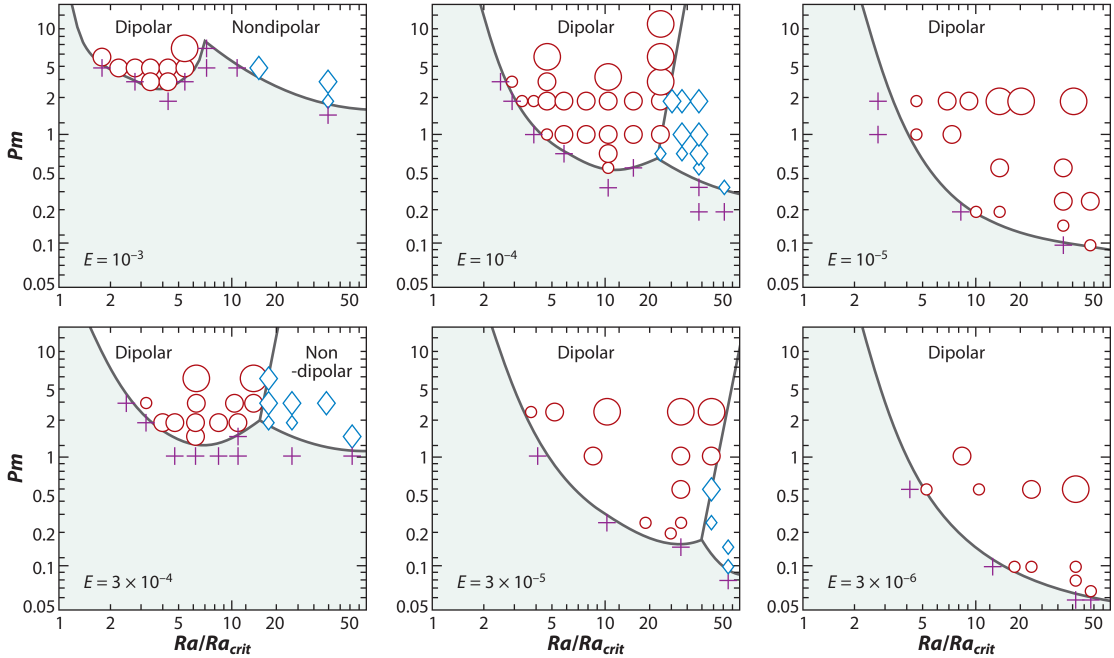

Figure 8

Regime diagram for dynamos as a function of Ra/Ra_c and Pm at six different values of E. $Pr = 1$ throughout. The area of the red circles scales with the strength of the field. Blue diamonds denote nondipolar dynamos, and purple crosses are failed dynamos. Figure reproduced with permission from Christensen & Aubert (2006).

concern as liquid metals have low Pm, typically in the range 10^{-5}–10^{-6}. However, optimism was restored when it was noted that as E is lowered, dynamos can be obtained with lower Pm (**Figure 8**). At $E = 10^{-4}$, $Pm = 0.5$ can be reached, and at $E = 3 \times 10^{-6}$ dynamos can be found at $Pm = 0.06$. There is no prospect of finding numerical dynamos at much lower Pm than this. Another notable feature shown in **Figure 8** is that at larger Ra, dipole-dominated dynamos are not found. A magnetic field is generated, but the field typically has no systematic large-scale components. The (small) dipolar component fluctuates, so these can be reversing dynamos. Near the border between the reversing dynamos and the dipolar dynamos, a great range of dynamical behavior is possible, including dynamos that are dipole dominated but occasionally reverse, which have been suggested as a possible model for reversals in the Earth's core (Olson & Christensen 2006), where the time between reversals is very much longer than the duration of individual reversals.

The border between these dipolar dynamos and the reversing dynamos is where the inertial terms in the equation of motion start to become important (Olson & Christensen 2006, Sreenivasan & Jones 2006a). An inertia-free limit is reached when Pm is increased while E and Ra are held fixed. To avoid affecting the relative strength of the thermal diffusion to advection ratio, Sreenivasan & Jones performed a series of runs at varying $Pr = Pm$ with $E = 10^{-4}$ and $Ra = 7.5 \times 10^6$. The magnetic Reynolds number and mean magnetic field were defined by

$$Rm = \frac{U_* d}{\eta}, \quad U_* = \left[\frac{1}{V} \int_V \mathbf{u}^2 \, dv \right]^{1/2}, \quad \overline{B} = \left[\frac{1}{V} \int_V \mathbf{B}^2 \, dv \right]^{1/2}, \tag{13}$$

where V is the volume of the outer core. **Figure 9*a*** shows the magnetic Reynolds number as a function of time on units of the magnetic diffusion time. In every case a saturation level is eventually

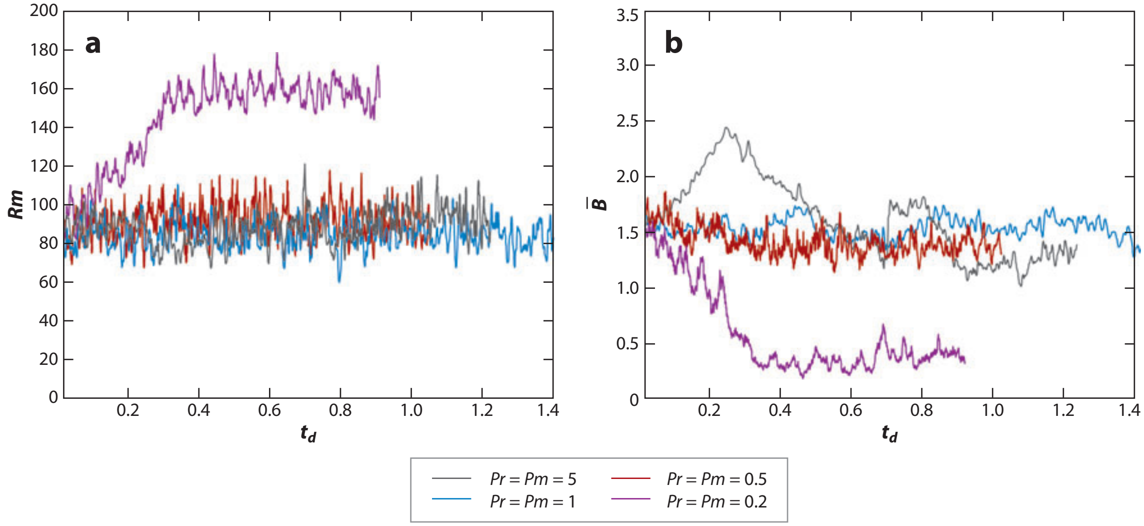

Figure 9

(*a*) Magnetic Reynolds number *Rm* plotted as a function of magnetic diffusion time and (*b*) mean magnetic field as a function of magnetic diffusion time. Figure taken with permission from Sreenivasan & Jones (2006a).

attained, which is fairly independent of $Pr = Pm$ provided $Pm \geq 0.5$, but Rm (and so the kinetic energy) is much larger at $Pr = Pm = 0.2$. Similarly, in **Figure 9*b*** the mean $\overline{B}$ is reasonably independent of Pm above 0.5 but is much lower when the inertial regime is reached. To establish that the transition is indeed connected with inertia, **Figure 10** plots the relative strength of the radial components of the Lorentz force $|(\nabla \times \mathbf{B}) \times \mathbf{B}|_r$, the Coriolis acceleration $|2\hat{\mathbf{z}} \times \mathbf{u}|_r$, and the advective part of the inertial acceleration $EPm^{-1}|(\nabla \times \mathbf{u}) \times \mathbf{u}|_r$ at a randomly chosen time, for points on half of a section parallel to the equatorial plane at $z = 0.5d$. It is clear that inertia is negligible at the higher Pm values, and Lorentz force is not, whereas at low Pm inertia is large and Lorentz force is comparatively unimportant in controlling the convection (although it must play a role in determining the low magnetic field strength). This inertia-free regime in which the main force balance is between the magnetic Lorentz force (M), the buoyancy, or Archimedean force (A), and the Coriolis acceleration (C). This regime is therefore known as the MAC balance, or the magnetostrophic, regime.

At low E, the dipolar dynamos develop a much finer velocity structure. **Figure 11*a*** shows an equatorial section of the radial velocity of a dynamo at $E = 3 \times 10^{-6}$, $Pr = 1$, and $Pm = 0.1$. The velocity is only weakly dependent on z, and the fluid motion is more in sheets than in columns. This type of flow has also been found at low E by Kageyama et al. (2008) in a slightly different model. As might be expected given the low Pm, magnetic diffusion is larger than viscous diffusion, and the magnetic field structures shown in **Figure 11*b*** are thicker than the velocity structures. This is perhaps the first clear evidence of scale separation between the size of the magnetic and fluid structures.

5.2. J.B. Taylor's Constraint

J.B. Taylor (1963) showed that if the force balance in the core was magnetostrophic, the magnetic field must satisfy a constraint. The ϕ component of momentum integrated over a cylinder radius

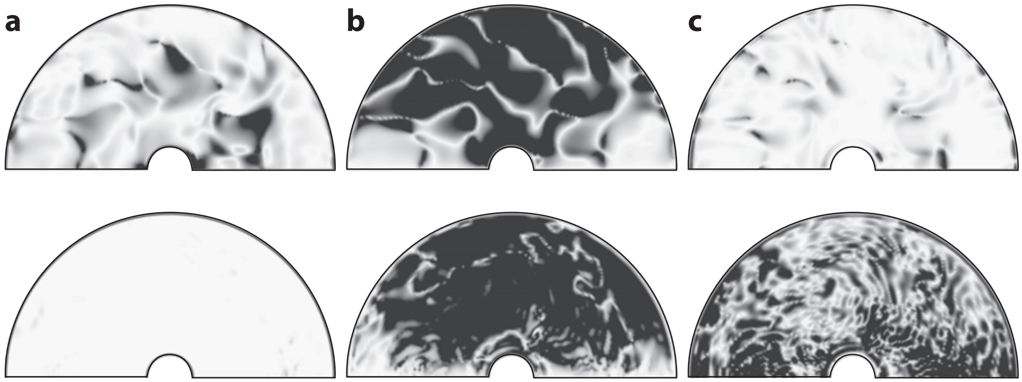

Figure 10

Relative strength of the radial component of the (*a*) Lorentz force, (*b*) Coriolis acceleration, and (*c*) inertial acceleration on a horizontal section at elevation $z = 0.5$ north of the equatorial plane. Only half the section is shown. The intensity of each point is the ratio of the magnitude of that force to the strongest force at that point. Each force is divided by the strongest of the forces at each point (including buoyancy and viscous forces, not shown) and is shaded black for a value near 1, and white for a value near 0. $Pr = Pm = 1$ (*top row*) and 0.2 (*bottom row*). Note that at $Pr = Pm = 1$, the Lorentz force is greater than inertial acceleration, but at $Pr = Pm = 0.2$, inertial acceleration is much larger than the Lorentz force. Figure taken with permission from Sreenivasan & Jones (2006a).

s cut off by the CMB gives (see, e.g., Fearn 1998)

$$\frac{\partial}{\partial t}\int_{C(s)} \rho u_\phi \, ds + \int_{C(s)} 2\rho u_s \Omega \, ds = \int_{C(s)} (\mathbf{j} \times \mathbf{B})_\phi \, ds - 4\pi s \frac{\rho u_\phi (\nu \Omega r_{cmb})^{1/2}}{(r_{cmb}^2 - s^2)^{1/4}}. \quad (14)$$

The Coriolis term is zero because there is no net flow across the cylinder, and buoyancy has no ϕ component. Reynolds stress is ignored because it is believed to be small in the core, although it is not small in many simulations. The last term comes from the viscous friction at the boundaries, which is produced by Ekman suction (e.g., Fearn 1998). It is small because E is small. On a

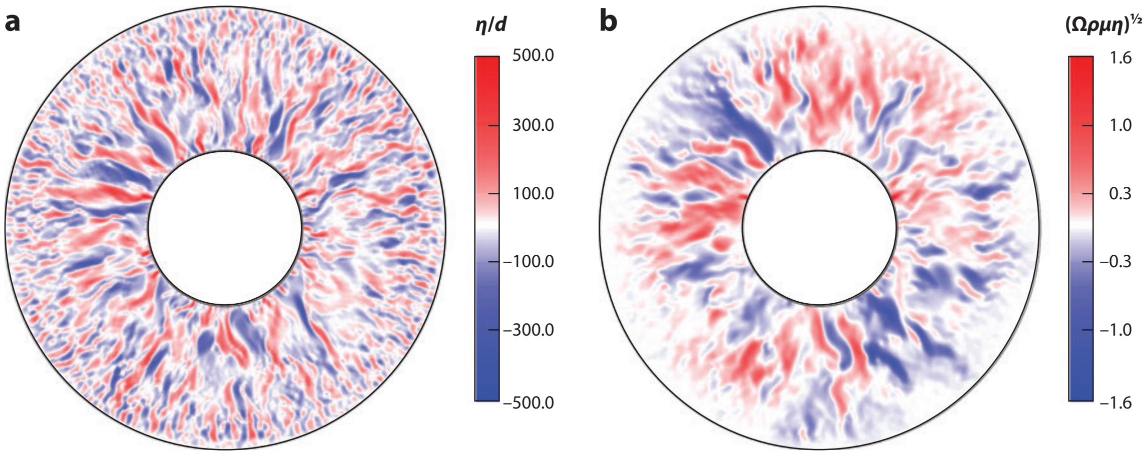

Figure 11

Snapshot of a dynamo simulation at $E = 3 \times 10^{-6}$, $Pr = 1$, $Pm = 0.1$, and $Ra = 2.33 \times 10^9$: (*a*) equatorial section of u_r and (*b*) equatorial section of B_r. The flow is quite independent of z and so consists of narrow sheets. The magnetic field structures have less very-small-scale structures, as expected at low Pm.

long-term average, the time-dependent term must be zero, so the Lorentz force balances the Ekman suction. Because this is small, but **B** and **j** are not, the magnetic field must be constrained to be in a special configuration that makes the integral almost zero, and this is Taylor's constraint. Low-E simulations (particularly plane-layer models, which can reach lower E) do seem to satisfy Taylor's constraint (Rotvig & Jones 2002). The degree to which Taylor's constraint is satisfied is monitored by the Taylorization parameter

$$\mathrm{Tay} = \frac{\int_{C(s)} \mathbf{j} \times \mathbf{B} \cdot \mathbf{1}_\phi dS}{\int_{C(s)} |\mathbf{j} \times \mathbf{B} \cdot \mathbf{1}_\phi \mid dS}. \tag{15}$$

Aubert (2005) reported that at low E the Taylorization parameter is becoming small in spherical dynamos, as did Christensen & Wicht (2007). Takahashi et al. (2005) also claimed to have found a quasi-Taylor state at low E.

Torsional oscillations of the Taylor cylinders about the magnetostrophic equilibrium, torsional Alfvén waves, have been reported in the core with a period of around 50 years (Zatman & Bloxham 1997). However, Gillet et al. (2010) have recently found a 6-year oscillation both in the secular variation of the magnetic field and in the length of the day, which they identify with a torsional oscillation. If this is correct, it would correspond to an root-mean-square field strength of about 4 mT in the core, considerably stronger than the field at the CMB (see **Figure 1*a***). This strong field is more consistent with current geodynamo models than the much weaker field implied by a 50-year torsional oscillation period. Possible excitation mechanisms are discussed by Dumberry & Bloxham (2003).

5.3. Stress-Free Boundaries

Stress-free boundaries are commonly used on the grounds that the effect of the Ekman boundary layers that occur in no-slip simulations is overestimated because the Ekman number is too large for numerical reasons, and it would therefore be better to remove the boundary layers altogether (Kuang & Bloxham 1997). Stress-free nonmagnetic convection simulations lead to much larger zonal flows (axisymmetric flow in the ϕ direction) than are found with no-slip boundaries, because the inertial Reynolds stresses only compete against the internal viscosity and not the much larger boundary layer friction. Consequently, inertial effects, and in particular the effect of zonal flow, are far more apparent in stress-free boundary cases. This leads to a rich dynamical behavior; it is possible to find quadrupolar dynamos (Simitev & Busse 2005, Busse & Simitev 2006), fluctuating dynamos (Simitev & Busse 2008), and even hemispherical dynamos, that is, dynamos predominantly in one hemisphere (see Grote & Busse 2000). This work was reviewed in Busse & Simitev (2007). The shear driven by the convection can disrupt the convection, and hence the dynamo. It is therefore possible to obtain regions of reduced shear, where the field and the convection are active, and regions dominated by shear, where convection is reduced and no field is generated. More recently, it has been noted that in this transition region, multiple steady solutions can be found; that is, with some initial conditions, dipolar dynamos can be found, but with other initial conditions, small-scale dynamos are found at exactly the same parameter values (Simitev & Busse 2009). Simply evaluating the strength of the inertial terms in the Earth's core suggests that they are very small compared with other terms, except over very short length scales [Sreenivasan & Jones (2006a) estimated length scales below 4 km], which are too small to affect the dynamo. Even small inertial terms can be significant in building zonal flow if they are opposed only by small viscous terms in the absence of a magnetic field, but large zonal flows seem unlikely in the presence of a magnetic field, although Miyagoshi et al. (2010) presented a low-E dynamo with a region of strong differential rotation outside the field-generating region.

5.4. Thermal Boundary Conditions and Internal Heating

The effect of changing the thermal boundary conditions and adding internal heating was investigated by Kutzner & Christensen (2002). They showed that adding internal heating reduces the dipole dominant region, whereas chemical convection (which acts like thermal convection with an effective heat sink in the outer core) extends the dipolar region (**Figure 12**). They found that changing from a constant-temperature boundary condition to a fixed-flux boundary condition made little difference, but Sakuraba & Roberts (2009) looked at low $E \sim 2 \times 10^{-6}$ (using our definition) and $Pm = 1$, $Pr = 0.2$, and found significant differences between fixed-flux and fixed-temperature boundary conditions. In particular, the flow structures are much broader with fixed-flux boundary conditions (see **Figure 13**), and in consequence flux patches on the CMB are more significant, as on the Earth. The very fine velocity structures seen in **Figures 11*a*** and **13*a*** lead to a much more dipolar field than the geomagnetic field. Sakuraba & Roberts attribute the difference to the large-scale flows driven by the temperature differences that appear on the CMB when fixed-flux conditions are used.

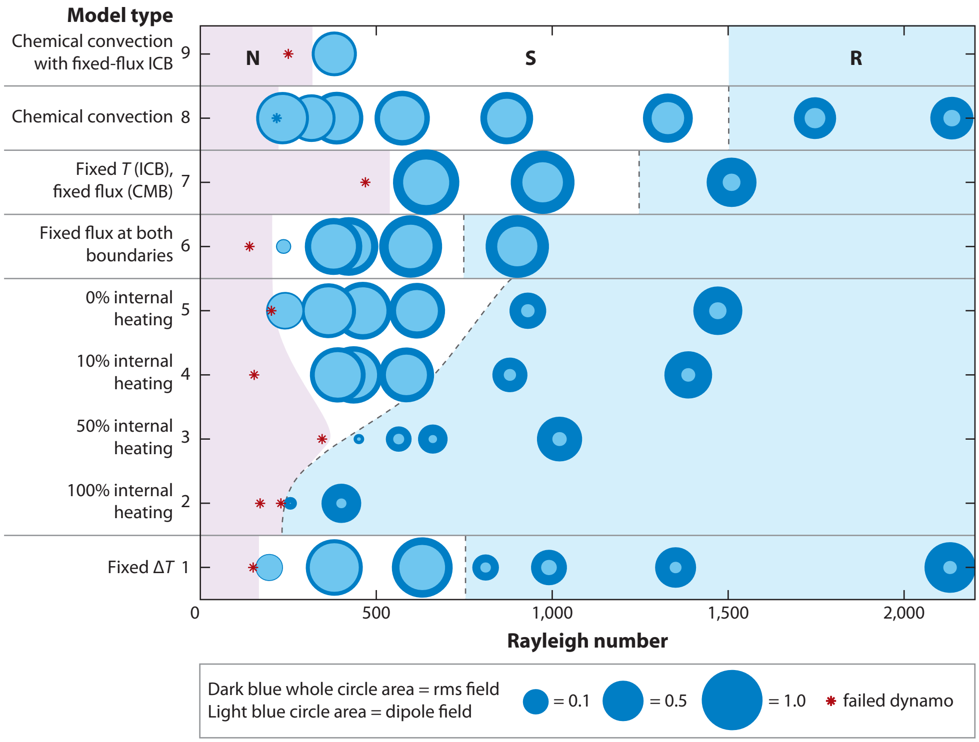

Figure 12

Dynamos found with varying boundary conditions and internal heating. $E = 3 \times 10^{-4}$, $q = Pm/Pr = 3$, and $Pr = 1$. The Rayleigh number on the scale is a factor E smaller than that defined here. N are regions of no dynamos, S are stable dipolar dynamos, and R are reversing nondipolar dynamos. The size of the circles relates to field strength. Abbreviations: CMB, core-mantle boundary; ICB, inner-core boundary. Figure reprinted from Kutzner & Christensen (2002), with permission from Elsevier.

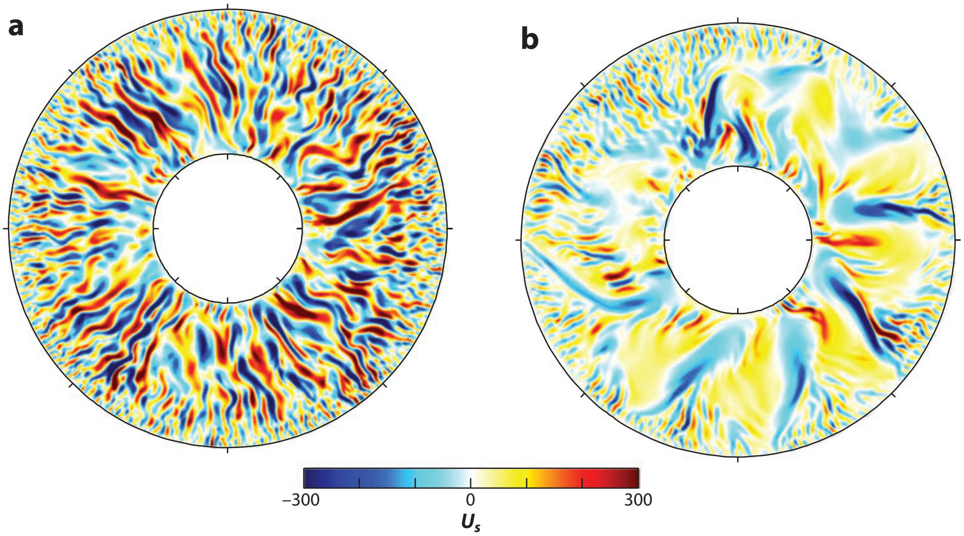

Figure 13

Equatorial section of $u_s = u_r$ for a dynamo at $E = 2.37 \times 10^{-6}$, $Pr = 1$, $Pm = 0.2$, and $Ra \sim 9 \times 10^9$ in the units used here: (*a*) constant temperature on the core-mantle boundary (CMB) and (*b*) constant heat flux on the CMB. The flow is quite independent of z, so the flow consists of narrow sheets. Note the larger-scale structures that appear in the constant–heat flux case. Figure reprinted by permission from Macmillan Publishers Ltd.: Sakuraba & Roberts (2009).

6. SCALING LAWS AND HEAT TRANSPORT

As we can never perform simulations at very small E and Pm, the hope is that we can identify the behavior in the asymptotic limit as $E \to 0$ and $Pm \to 0$ and hence evaluate the magnetic field strengths and velocities to be expected for given heat flux and boundary conditions. This asymptotic limit is described by scaling laws; the idea is that we will be able to perform a simulation at numerically possible values of E and Pm with the appropriate geometry, boundary conditions, and internal heating distribution and use the scaling laws to convert the output into numbers that can be compared directly with observations of the real planet. This is clearly an ambitious program, but some progress has been made.

Two complementary approaches are possible when deriving scaling laws. The direct approach, exemplified by Christensen & Aubert (2006), is to look at many dynamo model runs to see if asymptotic laws are emerging. The alternative (e.g., Starchenko & Jones 2002) is to use physical arguments to see which terms are balancing in the appropriate limit. This is not straightforward, because even if pressure forces are discounted by considering vorticity, there are still five terms in Equation 4, inertial and Coriolis accelerations balanced against buoyancy, Lorentz forces, and viscosity. We focus on the case of thermal driving only, but compositional convection can be dealt with by similar methods.

In nonlinear theories, the temperature fluctuation is estimated from the convected heat flux, given by a surface integral at constant r,

$$Q_{conv} = \int_S \rho c_p u_r T \, dS \sim 4\pi r_{icb} r_{cmb} \rho c_p U_* T_*, \tag{16}$$

where U_* and T_* are the typical velocity and temperature fluctuations, defined in simulations by the volume integrals over the outer core

$$U_* = \left[\frac{1}{V}\int \mathbf{u}^2\,dv\right]^{1/2} \qquad T_* = \left[\frac{1}{V}\int T^2\,dv\right]^{1/2}, \tag{17}$$

and c_p is the specific heat. Recall that T here is the very small superadiabatic temperature, not the actual temperature. The symbol $\sim$ here means there is a numerical constant of proportionality that can be determined by a simulation. The choice $4\pi r_{icb} r_{cmb}$ follows Christensen & Aubert (2006). The hope here (and below) is that the same constant will serve for all solutions with the same geometry and boundary conditions. This assumes that there is a strong constant correlation between hot fluid and rising fluid. In rotating convection this is not so clear, but the limited numerical evidence we possess does give it some support. Note that in a strongly convecting steady state with no heat sources, the total heat flux is independent of r, and so outside of boundary layers, Q_{conv} will also be independent of r. Astrophysicists use mixing-length theory, a balance between inertia and buoyancy,

$$U_*^2/d \sim g\alpha T_* \sim \frac{g\alpha Q_{conv}}{4\pi r_{icb} r_{cmb}\rho c_p U_*}. \tag{18}$$

In compressible convection, d is usually taken as the density-scale height, and in Boussinesq convection as the distance between the boundaries. The typical velocity is then the Deardorff velocity

$$U_* \sim \left(\frac{g\alpha Q_{conv} d}{4\pi r_{icb} r_{cmb}\rho c_p}\right)^{1/3}. \tag{19}$$

The plane-layer version of this works well in laboratory experiments. In the core, for 1 TW of convective heat flux, $\rho \approx 10^4$ ms^{-1}, $c_p \sim 900$ Jkg^{-1} K^{-1}, $g \approx 8$ ms^{-2}, and $\alpha \approx 10^{-5}$ K^{-1}, this gives U_* about 10 times too big, suggesting that rotation and magnetic field are slowing down the convection.

6.1. Inertial Theory of Rotating Convection

The essential modification for rotating convection is to allow for tall thin columns, involving the new short length scale, the column width $L_\perp$. The vorticity ($\boldsymbol{\omega}$) equation, ignoring viscosity, gives

$$\frac{D\boldsymbol{\omega}}{Dt} - 2(\boldsymbol{\Omega}\cdot\nabla)\mathbf{u} = \nabla\times g\alpha T\,\hat{\mathbf{r}} + \frac{1}{\rho}\nabla\times(\mathbf{j}\times\mathbf{B}). \tag{20}$$

Ignoring (temporarily) the Lorentz force, this suggests that the order-of-magnitude balance is

$$\frac{U_*^2}{L_\perp^2} \sim \frac{\Omega U_*}{d} \sim \frac{g\alpha T_*}{L_\perp}, \tag{21}$$

where the magnitude of the vorticity is $U_*/L_\perp$. The first term comes from nonlinear vorticity advection over the short length scale $L_\perp$, and the second term comes from the stretching of the planetary vorticity over the long length scale d due to the motion along the sloping boundaries. Then

$$L_\perp \sim \left(\frac{U_* d}{\Omega}\right)^{1/2} \sim \left(\frac{5\times10^{-4}\times2\times10^{6}}{7\times10^{-5}}\right)^{1/2} \sim 4\,\text{km}, \tag{22}$$

where $L_\perp$ is Rhines length, the length scale at which there is a balance of inertial and Coriolis accelerations. On longer length scales, inertial acceleration is small compared with Coriolis acceleration.

As in mixing-length theory, we use Equation 16 to eliminate T_*, and from Equation 21

$$L_\perp \sim d\left(\frac{g\alpha Q_{conv}}{4\pi r_{icb} r_{cmb} \Omega^3 d^2 \rho c_p}\right)^{1/5}, \tag{23a}$$

$$g\alpha T_* \sim \left(\frac{\Omega}{d}\right)^{1/5}\left(\frac{g\alpha Q_{conv}}{4\pi r_{icb} r_{cmb} \rho c_p}\right)^{3/5}, \tag{23b}$$

$$\frac{U_*}{\Omega d} = Ro \sim \left(\frac{g\alpha Q_{conv}}{4\pi r_{icb} r_{cmb} \rho c_p \Omega^3 d^2}\right)^{2/5}. \tag{24}$$

Hide (1974) and Ingersoll & Pollard (1982) proposed these scalings, and they were tested experimentally by Aubert et al. (2001). Gillet & Jones (2006) studied them numerically, using the quasi-geostrophic approximation, that is, assuming the vorticity parallel to z is independent of z. For compositional convection, Q_{conv} is replaced by the compositional buoyancy flux. Christensen & Aubert (2006) defined a flux Rayleigh number

$$Ra_Q = \frac{g\alpha Q_{conv}}{4\pi r_{icb} r_{cmb} \rho c_p \Omega^3 d^2}. \tag{25}$$

Fitting data from dynamo simulations, they obtained

$$Ro = 0.83\, Ra_Q^{0.41}, \tag{26}$$

which is very close to Equation 24, the inertial scaling. Taking the typical core velocity as 15 km per year from the secular variation gives $Ro = U_*/\Omega d = 2.9 \times 10^{-6}$, giving

$$Ra_Q \sim 2 \times 10^{-14} \rightarrow Q_{conv} \sim 0.6\,\mathrm{TW}. \tag{27}$$

This is a reasonable value consistent with independently obtained estimates of the total heat flux. Compositional convection may be releasing a mass flux of 3×10^4 kgs^{-1} at the ICB, which would be equivalent to $Ra_Q \sim 8 \times 10^{-13}$. This would give a rather high value for the typical velocity in the core, 60 km per year.

One problem with Equations 23 and 24 is that they predict that $L_\perp$ has a very small value of about 4 km in the core. If we assume that the magnetic field prevents $L_\perp$ from becoming this small, a fixed value of $L_\perp$ rather than that given in Equation 23a leads to an exponent of 1/2 rather than 2/5 in Equation 24, as suggested by Starchenko & Jones (2002). This would give a slightly lower velocity for the given compositional mass flux.

6.2. Magnetic Field Strength

In the Earth's core, magnetic energy is much greater than kinetic energy, so a simple equipartition as used in astrophysics will not work here. One approach (Christensen & Aubert 2006) to estimating the field strength is through estimating the rate of ohmic dissipation. The rate of working of the buoyancy force equals the rate of ohmic and viscous dissipation in a steady state. We denote the fraction of ohmic dissipation to the total dissipation as f_{ohm}. In dynamo models the rate of ohmic dissipation is typically similar to the rate of viscous dissipation, $f_{ohm} \approx 0.5$, but the low Pm suggests a value closer to unity might be more appropriate in the core. We can estimate the buoyancy force work in terms of the heat flux by taking the scalar product of Equation 4 with **u** and integrating over the whole outer core, so

$$\int \eta\mu \mathbf{j}^2\, dv = f_{ohm} \int \frac{g\alpha}{c_p}\left[\int \rho c_p u_r T'\, dS\right] dr \approx 7.01\, f_{ohm} \rho \Omega^3 d^5 Ra_Q \tag{28}$$

for the geometry of the Earth's core (Christensen & Aubert 2006).

Now we need to relate the magnetic energy to ohmic dissipation. The dissipation time is the time taken for the magnetic energy to be dissipated through ohmic loss, which for a solid conductor would scale as d^2/η. For a whole sphere of radius a, Moffatt (1978) gave the e-folding time as $\tau_{diss} = a^2/\pi^2\eta$. Christensen & Tilgner (2004) proposed that in a turbulent fluid, this time would be reduced by a factor Rm, the magnetic Reynolds number, so then $\tau_{diss} \sim d/U_*$, independent of η. Equivalently, we can think of the dissipation taking place over a short length scale $d\,Rm^{-1/2}$, which is the expected length scale if the magnetic field is concentrated into flux ropes (Galloway et al. 1977), which then dominate the dissipation. Then

$$\int \eta\mu\mathbf{j}^2\,dv \sim \frac{Rm\eta}{d^2}\int \mathbf{B}^2/2\mu\,dv. \tag{29}$$

We now have

$$\int \eta\mu\mathbf{j}^2\,dv \sim \frac{U_*}{d}\int \frac{\mathbf{B}^2}{\mu}dv \sim f_{ohm}\rho\Omega^3 d^5\,Ra_Q. \tag{30}$$

Using Equation 24 to estimate U_*, this gives

$$B_* \sim (\mu f_{ohm}\rho)^{1/2}\Omega d(Ra_Q)^{3/10} \sim (\mu f_{ohm})^{1/2} d^{-1/5}\rho^{1/5}\Omega^{1/10}\left(\frac{g\alpha Q_{conv}}{c_p}\right)^{0.3}. \tag{31}$$

The remarkable feature is the weak dependence of B_* on Ω. We are assuming, however, that the planet is in the rapidly rotating low Ro regime for these estimates to be plausible. This estimate does give sensible field strengths for the Earth and Jupiter (Christensen & Aubert 2006), the two planets for which we have reasonable estimates for the heat flux and the other physical quantities in the formula.

It is not easy to reconcile Equation 31 with the balance in the vorticity equation given in Equation 20, which is slightly worrying as the fundamental MAC balance in the core is believed to be between the buoyancy force, Lorentz force, and Coriolis acceleration. The simplest estimate for the Lorentz force in Equation 20 is $B_*^2/\mu L_\perp^2$, and balancing this against the Coriolis estimate $\rho\Omega U_*/d$ gives

$$B_* \sim (\mu\rho)^{1/2}\Omega d\,Ra_Q^{2/5}, \tag{32}$$

slightly different from Equation 31 and significantly smaller in the core. A more detailed model would be to balance the buoyant driving and vortex stretching in the z-vorticity equation with the magnetic friction torque from the B_ϕ component of the magnetic field. One might reasonably assume that the length scale $L_\perp$ is set by the balance of induction and diffusion in the induction equation, leading to $B_*U_* \sim \eta\mu j_*$, which in the vorticity equation gives

$$B_* \sim (\Omega\rho\mu\eta)^{1/2}\left(\frac{L_\perp}{d}\right)^{1/2}. \tag{33}$$

In the range of simulations, none of the three estimates given in Equations 31–33 is very different, and each depends on how $L_\perp$ scales at low Ra_Q, which is unclear because, as mentioned above, it seems unlikely that Equation 23a continues to be valid in the asymptotic limit. It is also worth noting that Equation 31 estimates B_* from the total magnetic energy rather than the average of the modulus of the field. At large Rm there may be concentrated flux ropes at which the field is locally much larger than its typical value. The magnetic energy $\mathbf{B}^2/\mu$ is then dominated by these flux ropes, and the estimate given in Equation 31 would be significantly larger than the typical value outside the ropes. The estimate given in Equation 33, alternatively, might relate to the lowest values of the B_ϕ field, where the magnetic damping of the convective rolls is weaker. It is clear that more work needs to be done before we can be confident about the correct scaling laws, but nevertheless an encouraging start has been made.

7. MODELS OF THE MAGNETIC FIELDS OF INDIVIDUAL PLANETS

7.1. Mercury

Mercury has a radius of only 2,440 km, but it has a relatively large fluid core, with a radius of about 1,900 km. Space missions have enabled the dipole moment, 4.2×10^{12} Tm^3, and the low-order Gauss coefficients to be determined (Uno et al. 2009), and the radial component of the field at the CMB is shown in **Figure 14**. The field pattern is not too dissimilar from the geomagnetic field truncated at degree 3, but the field strength is about 500 times weaker than the Earth's CMB field. This difference has been considered to result from Mercury's slow rotation period, 59 days, but the more recent view is that field strength is only weakly dependent on rotation, provided the Rossby number is small. Two dynamo models accounting for Mercury's weak field have been proposed. Christensen (2006) suggested that only the deepest part of Mercury's outer core is convecting; the upper parts may be stably stratified [as has been proposed for the Earth by Willis et al. (2007), although Mercury's stable layer is assumed much deeper]. The dynamo in the lower core is then operating in essentially the same way as the geodynamo, but the stable conducting regions only allow a small fraction of the field to escape to the surface, and they filter out all the high-degree harmonics. Hence the observed field of Mercury appears much weaker. An alternative thin-shell model was proposed by Stanley et al. (2005). Compositional convection may be more advanced in Mercury, leaving only a thin shell of liquid with a high concentration of light material, the rest being solid iron. A thin-shell dynamo would have more power in the higher harmonics, not observable (so far) from space missions, and a relatively weak dipolar component. Also they argue that the ω-effect could be more important in thin-shell dynamos, with the field being limited by a large unobservable toroidal component. As these two theories make quite different predictions for the magnetic spectrum, the new missions to Mercury might help decide between them.

7.2. Earth

There is a large literature on models of the Earth's magnetic field, a good source being volume 5 of the *Treatise of Geophysics* edited by Kono (2007). Here we briefly overview a selection of topics that have attracted attention recently.

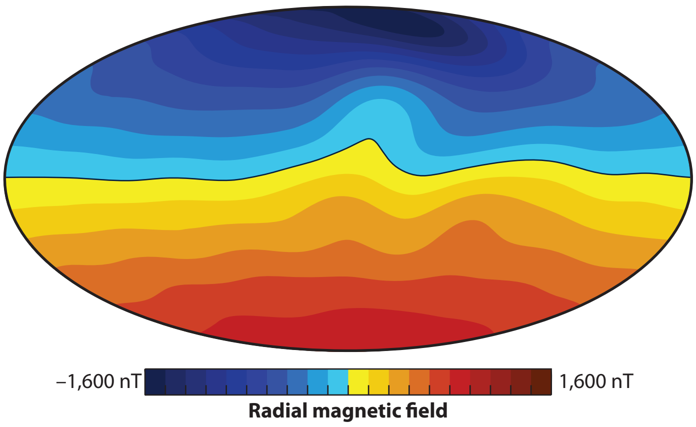

Figure 14

The radial component of Mercury's magnetic field at its core-mantle boundary, centered on longitude zero.

7.2.1. Polar vortices. Dynamo models often show a significant difference between the polar regions inside the tangent cylinder and the rest of the outer core, a consequence of the columnar structure of the convection. Olson & Aurnou (1999) found geomagnetic evidence that the polar regions have an anticyclonic vortex. They suggested this might be due to excess heat and light material released from the ICB. From the thermal wind equation, the ϕ component of the vorticity equation,

$$2\Omega \frac{\partial u_\phi}{\partial z} = \frac{g\alpha}{r} \frac{\partial T}{\partial \theta}, \tag{34}$$

the resulting latitudinal temperature gradient (or composition gradient) makes the flow anticyclonic near the CMB and cyclonic near the ICB. Glatzmaier & Roberts (1996a) proposed that this might mean that the inner core is rotating slightly faster than the mantle, for which there has been some seismological evidence. More recently, this inner-core super-rotation has been questioned, and Buffett & Glatzmaier (2000) suggested that gravitational coupling between a slightly nonaxisymmetric inner core and mantle might in fact lock the rotation of the inner core to the mantle. Aurnou et al. (2003) showed that polar vortices of the correct sign of vorticity could be produced in laboratory convection with a hemispherical inner core. Sreenivasan & Jones (2005, 2006b) found polar vortices in dynamo simulations but noted that the Lorentz force played a significant role in the thermal wind equation.

7.2.2. History of the geodynamo and reversals. Models of the thermal history of the Earth suggest that the inner core only started forming about 1 Gyr ago (Labrosse et al. 2001), much less than the age of the Earth, 4.5 Gyr. Because the inner core generates most of the heat flux and all the mass flux in the standard model, Roberts et al. (2003) suggested that there must be radioactivity in the core to provide the heat flux necessary to drive the dynamo prior to inner-core formation. Paleomagnetic evidence suggests that the dynamo has been working at more or less its present strength for at least 3.5 Gyr. Aubert et al. (2009) have examined the secular changes in dynamo activity as heat and composition sources evolve.

Glatzmaier & Roberts (1995) found a dynamo that had quite earthlike reversals. Sarson & Jones (1999) analyzed a reversing dynamo and suggested that the origin of the reversals lay in fluid breaking out of the thermal boundary layer near the ICB, giving rise to buoyancy surges. Large *Ra* was necessary for this to occur, which is numerically difficult. Kutzner & Christensen (2004) explored earthlike reversals near the transition between the inertia and inertia-free regimes, an idea developed by Olson & Christensen (2006), who gave criteria for a dynamo to be in this reversing regime.

7.2.3. Mantle heterogeneity. The heat flux taken out of the core by the mantle is likely to vary strongly with position, being highest where cool descending slabs from subducting plates reach the CMB. This heterogeneity can be estimated using seismic tomography (see, e.g., Gubbins et al. 2007) and will couple dynamo activity in the core to long geological timescales. Glatzmaier et al. (1999) found that reversals in dynamo models were strongly affected by the distribution of heat flux over the CMB, with some arrangements preventing reversals and others encouraging them. They proposed that the long Cretaceous superchron, 40 Myr during which there were no reversals, resulted from mantle convection giving rise to a CMB heat flux distribution that suppressed reversals. Heterogeneous CMB heat flux has also been proposed as an explanation for the preferred reversal paths noted by Hoffman (1992) and the persistent flux patches over Canada and Siberia (Gubbins & Kelly 1993). The effects of heterogeneous CMB heat flux on dynamo models have been investigated by Willis et al. (2007). Mantle inhomogeneity might affect convection throughout the outer core, and hence lead to inhomogeneity in the way freezing takes place at the ICB (Aubert et al. 2008a).

7.3. Mars

The Mars Global Surveyor discovered strong remanent magnetism on Mars (Acuña et al. 2001), suggesting that it had an ancient dynamo. The age at which it stopped working, around 350 Myr after the formation of the planet, can be estimated by studying the geology of Mars (Lillis et al. 2008). It is known that Mars still has a liquid core (Yoder et al. 2003), so the simplest explanation is that the core stopped convecting and hence the power source failed. Kuang et al. (2008) used a dynamo model to show that a dynamo can collapse quite suddenly, due to its subcritical nature. The martian magnetic field is predominantly in one hemisphere, which led Stanley et al. (2008) to propose a model based on an asymmetric convection pattern, which might have been induced by the crustal asymmetry of that planet, the northern hemisphere crust being significantly thinner than that of the southern hemisphere uplands.

7.4. Ganymede

Ganymede's magnetic field was discovered by the Galileo spacecraft (Kivelson et al. 1996). The first problem was whether this was a genuine dynamo or merely an amplifier of Jupiter's magnetic field. Models by Sarson et al. (1997) concluded that a dynamo was more likely. Ganymede has an icy crust, a warm silicate mantle, and a metallic core. The radius is 2,634 km, but the metallic core radius is believed to be (from gravity measurements) approximately 500 km. The dipole moment is 1.3×10^{13} Tm^3, about three times larger than that of Mercury. At the surface the field is typically 700 nT, but at the CMB this rises to 0.12 mT, weaker than the Earth's CMB field but much stronger than Mercury's field. The outstanding problem with the Ganymede dynamo is the energy source. It is surprising that such a small body is still convecting; Showman et al. (1997) suggested that orbital resonances might lead to tidal heating, but this is still controversial (Bland et al. 2008). If Ganymede does indeed have a dynamo, it raises the interesting question of how small a planetary body can be and still have a dynamo. The recent discovery of microtesla magnetic fields on angrites (Weiss et al. 2008), meteorites that record the earliest history of the solar system, suggests that planetesimal components that subsequently formed the planets might have had their own dynamos.

7.5. The Giant Planets

All the outer planets are believed to be transporting heat by convection, so fluid motion is expected in their interiors. The very high pressures found in Jupiter and Saturn lead to metallic hydrogen; that is, the gas becomes ionized and hence electrically conducting. This electrical conductivity rises gradually with depth, reaching a plateau of 2×10^5 Sm^{-1} (Nellis 2000), three times lower than the usual estimate for the Earth's metallic core, 6×10^5 Sm^{-1} (see, e.g., Merrill et al. 1996). In Jupiter, the plateau is reached at a radius about 0.8 R_J, whereas in smaller Saturn, where the high pressures needed are found only deeper, it is reached at about 0.5 R_S. The Gauss coefficients for Jupiter and Saturn up to degree 3 are reconstructed from space-mission results, and are listed in Connerney (1993). There is some doubt as to where the dynamo is actually operating in the giant planets, because the overall magnetic Reynolds number is large, and it may be that dynamo action works best at moderate Rm. If this is true, regions where the electrical conductivity is below its maximum value may be optimal, in which case the magnetic region could extend above 0.8 R_J and

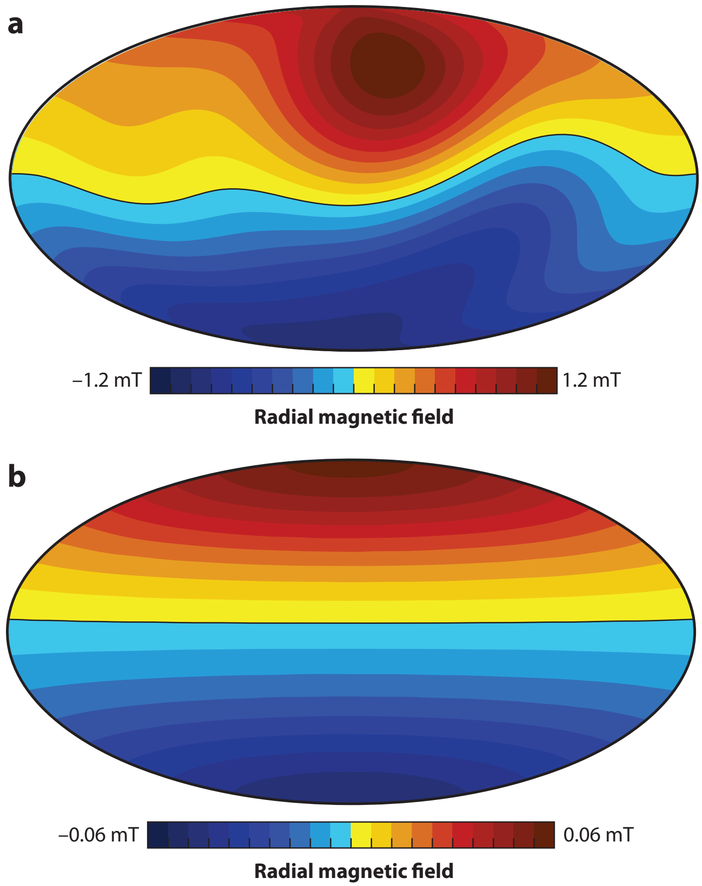

Figure 15

The radial component of (*a*) Jupiter's magnetic field and (*b*) Saturn's magnetic field, both at the surface using the Hammer-Aitoff projection, centered on longitude −180° west.

0.5 R_S. **Figures 15*a*,*b*** show the magnetic fields of Jupiter and Saturn at their surface. Jupiter's field (based on the Gauss coefficients given in Connerney 1993) is essentially a dipolar field inclined at about 10° to the rotation axis, similar to the Earth. Jupiter's rotation rate is defined by the rotation period of its magnetic field, which is accurately known. The surface features rotate at different rates depending on their latitude. This observation alone suggests that the typical convective velocity in the deep interior must be much less than the fast east-west jet flows at the surface, which can reach over 100 ms^{-1} in Jupiter and 300 ms^{-1} in Saturn. Observations of changes in the magnetic field of Jupiter between the Voyager and Galileo missions suggest flows on the order of 10^{-3} ms^{-1} are moving the field around (Russell et al. 2001).

As is clear from **Figure 15*b***, Saturn's magnetic field (based on the Gauss coefficients given in Burton et al. 2009) is remarkably axisymmetric, so much so that its rotation period cannot be reliably determined from its magnetic field, so the rotation rate of Saturn's deep interior is still uncertain. Saturn's field is also significantly weaker than Jupiter's field, but it should be remembered that the metallic hydrogen region in Saturn is at a depth of half its radius, so the field at its effective CMB could be nearly 10 times larger. Cowling's (1934) theorem tells us that axisymmetric fields cannot be generated by dynamo action, so assuming the dynamo hypothesis is correct, the generated field must be nonaxisymmetric, but processes outside the main dynamo region must be making the observed part of the field axisymmetric. Stevenson (1982) suggested that differential rotation in a stably stratified region outside the dynamo-generating core might be responsible, an idea supported by numerical simulations including a stably stratified outer layer (Christensen & Wicht 2008).

7.6. The Ice Giants

Uranus and Neptune both have rather irregular nondipolar fields, as illustrated in **Figure 16**. This was a quite surprising discovery as all previously known planetary fields were essentially dipolar. Indeed, it is quite surprising that these ice giants have a magnetic field at all, as they are too small to form metallic hydrogen and have no liquid-iron core. It is believed that ionic conductivity in the fluid ionic layer between 0.3 R_s and 0.8 R_s allows sufficient electric currents to flow (Cavazzoni et al. 1999). However, the predicted electrical conductivity is only 3×10^3 S m^{-1}, which does lead to an uncomfortably small magnetic Reynolds number unless the fluid velocities in the dynamo

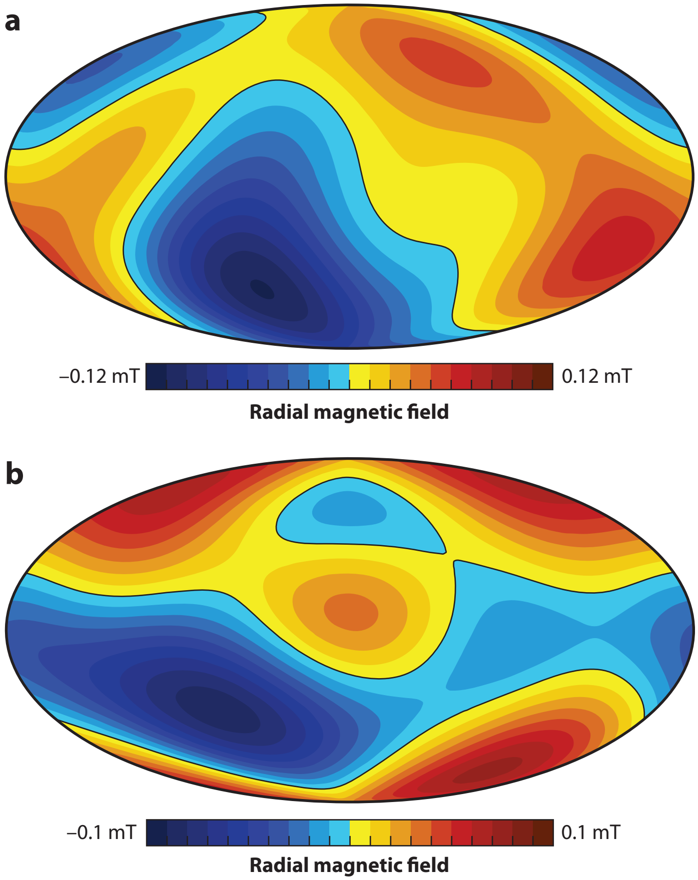

Figure 16

The radial component of (*a*) Uranus's magnetic field and (*b*) Neptune's magnetic field, both at the surface using the Hammer-Aitoff projection, centered on longitude −180° west. Data taken from Holme & Bloxham (1996).

region are significantly larger than those in other planetary cores. The difficulty is compounded in the case of Uranus by the small heat flux emerging from the planet, which if taken at face value would suggest a smaller convective velocity rather than a larger one. A further problem is that the ohmic dissipation in these ice giants turns out to be quite large (Holme & Bloxham 1996). Nevertheless, a dynamo model has been constructed (Stanley & Bloxham 2006). Their model has a stably stratified layer below the main dynamo region, which might also account for the low heat flux. This region allows the generated field to move around more than in models with a solid inner core, and this gives rise to nondipolar fields.

8. PERSPECTIVES AND FUTURE DEVELOPMENTS

Dynamo models have developed rapidly over the past 10 years, and the early successes in simulating the geodynamo have developed into quite detailed models of the magnetic fields of other planets. There is now a much greater coverage of the parameter space in the models, and the effects of varying driving, boundary conditions and parameter values are beginning to be understood. It is clear that a great diversity of behavior can arise in the models, but this is consistent with the diversity of planetary magnetic fields themselves. Another encouraging development is that the physical mechanisms behind dynamo action in the simulations are becoming better understood. Until recently, the numerical codes were essentially black boxes giving rather unpredictable results for each new parameter set. This encouraged researchers to adjust parameters, often motivated by numerical rather than physical reasons, until they found the behavior they wanted. This era does seem to be coming to an end, with the simulations now being used as a tool to explore new physical ideas relevant to planetary cores.

For the geodynamo, observations have given us a data set of the geomagnetic field over the past 300 years, with high-accuracy values over the past 30 years. Work is currently in progress to try to assimilate this data into geodynamo models (Gillet et al. 2009). The immediate aim here is to use this data to discriminate between different dynamo models. The dynamo model is thus a given prior, to which noisy observational data are added, the output being a time-dependent model of the geomagnetic field. A poor dynamo model leads to large residuals, a better model to smaller residuals. Ultimately, it may be possible to use these techniques to forecast the geomagnetic field (Kuang et al. 2009), but it is in the nature of the geodynamo equations (as it is with weather forecasting) that predictions far into the future will not be possible (Hulot et al. 2010).

We cannot, and probably never will be able to, use the true very low values of the dissipation in simulations. This problem is being overcome by understanding how the models behave in the asymptotic limit, the scaling-law approach, and although much remains to be done, the path ahead seems clear. However, the models that emerge as new computational resources allow us to move into the low-E, low-inertia, regime are if anything becoming less earthlike than the moderate $E \sim 10^{-4}$ solutions, which were the lowest that could be reached 10 years ago. In particular, recent low-E models are often very dipole dominant and show no prospect of reversing. It is too soon to say that there must be something fundamentally wrong with our overall physical picture; it is possible that higher Rayleigh numbers, better boundary conditions, improved modeling, and possibly compressible effects will give more earthlike behavior. It is also true that numerical constraints can be quite insidious, in that they force us into particular parameter regimes, leading to a false impression of the overall behavior. However, our improving understanding of dynamo processes and spherical convection may well make it possible to develop physically based earthlike models in the near future.

The general outlook for the subject remains extremely promising. New models of giant planet dynamos are ripe for progress, and the development of compressible planetary dynamo models is a major area for future research. There is a real possibility of discovering magnetic fields on exoplanets, which would give a huge new impetus to the subject. Analysis of magnetic fields in the remnants of the forming solar system may also help us to understand the origin of our planets.

DISCLOSURE STATEMENT

The author is not aware of any affiliations, memberships, funding, or financial holdings that might be perceived as affecting the objectivity of this review.

ACKNOWLEDGMENTS

I would like to thank Binod Sreenivasan, David Gubbins, and Phil Livermore for many useful discussions, which helped the preparation of this article. I am also grateful to Richard Holme, Uli Christensen, and Ataru Sakuraba for providing original figures. Thanks are due to the Leverhulme Trust, for providing support through grant F/00122/AD.

LITERATURE CITED

Acuña MH, Connerney JE, Ness NF, Lin RP, Mitchell D, et al. 1999. Global distribution of crustal magnetization discovered by the Mars Global Surveyor MAG/ER experiment. *Science* 284:790–93

Anufriev AP, Jones CA, Soward AM. 2005. The Boussinesq and anelastic liquid approximations for convection in the Earth's core. *Phys. Earth Planet. Inter.* 152:163–90

Aubert J. 2005. Steady zonal flows in spherical shell dynamos. *J. Fluid Mech.* 542:53–67

Aubert J, Amit H, Hulot G, Olson P. 2008a. Thermochemical flows couple the Earth's inner core growth to mantle heterogeneity. *Nature* 454:758–61

Aubert J, Aurnou J, Wicht J. 2008b. The magnetic structure of convection-driven numerical dynamos. *Geophys. J. Int.* 172:945–56

Aubert J, Brito D, Nataf H-C, Cardin P, Masson J-P. 2001. A systematic experimental study of rapidly rotating spherical convection in water and liquid gallium. *Phys. Earth Planet. Inter.* 128:51–74

Aubert J, Labrosse S, Poitou C. 2009. Modelling the palaeo-evolution of the geodynamo. *Geophys. J. Int.* 179:1414–28

Aurnou J, Andreadis S, Zhu L, Olson P. 2003. Experiments on convection in Earth's core tangent cylinder. *Earth Planet. Sci. Lett.* 212:119–34

Bland MT, Showman AP, Tobie G. 2008. The production of Ganymede's magnetic field. *Icarus* 198:384–99

Braginsky SI, Meytlis VP. 1990. Local turbulence in the Earth's core. *Geophys. Astrophys. Fluid Dyn.* 55:71–87

Braginsky SI, Roberts PH. 1995. Equations governing convection in Earth's core and the geodynamo. *Geophys. Astrophys. Fluid Dyn.* 79:1–97

Buffett BA, Glatzmaier GA. 2000. Gravitational braking of inner-core rotation in geodynamo simulations. *Geophys. Res. Lett.* 27:3125–28

Bullard EC. 1949. The magnetic field within the Earth. *Proc. R. Soc. Lond. A* 197:433–53

Burton ME, Dougherty MK, Russell CT. 2009. Model of Saturn's internal planetary magnetic field based on Cassini observations. *Planet. Space Sci.* 57:1706–13

Busse FH. 1970. Thermal instabilities in rapidly rotating systems. *J. Fluid Mech.* 44:441–60

Busse FH. 2000. Homogeneous dynamos in planetary cores and in the laboratory. *Annu. Rev. Fluid Mech.* 32:383–408

Busse FH, Simitev RD. 2006. Parameter dependences of convection-driven dynamos in rotating spherical fluid shells. *Geophys. Astrophys. Fluid Dyn.* 100:341–61

Busse FH, Simitev RD. 2007. Planetary dynamos. In *Treatise on Geophysics*, Vol. 10, ed. T Spohn, pp. 281–98. Amsterdam: Elsevier

Cavazzoni C, Chiarotti GL, Scandolo S, Tosatti E, Bernasconi M, Parrinello M. 1999. Superionic and metallic states of water and ammonia at giant planet conditions. *Science* 283:44–46

Christensen UR. 2006. A deep dynamo generating Mercury's magnetic field. *Nature* 444:1056–58

Christensen UR, Aubert J. 2006. Scaling properties of convection-driven dynamos in rotating spherical shells and application to planetary magnetic fields. *Geophys. J. Int.* 166:97–114

Christensen UR, Aubert J, Cardin P, Dormy E, Gibbons S, et al. 2001. A numerical dynamo benchmark. *Phys. Earth Planet. Inter.* 128:25–34

Christensen UR, Olson P, Glatzmaier GA. 1999. Numerical modeling of the geodynamo: a systematic parameter study. *Geophys. J. Int.* 138:393–409

Christensen UR, Tilgner A. 2004. Power requirement of the geodynamo from ohmic losses in numerical and laboratory dynamos. *Nature* 429:169–71

Christensen UR, Wicht J. 2007. Numerical dynamo simulations. See Olson 2007, pp. 245–82

Christensen UR, Wicht J. 2008. Models of magnetic field generation in partly stable planetary cores: applications to Mercury and Saturn. *Icarus* 196:16–34

Clune TC, Elliot JR, Miesch MS, Toomre J, Glatzmaier GA. 1999. Computational aspects of a code to study rotating turbulent convection in spherical shells. *Parallel Comput.* 25:361–80

Connerney JEP. 1993. Magnetic fields of the outer planets. *J. Geophys. Res. Planets* 98:18659–79

Cowling TG. 1934. The magnetic field of sunspots. *MNRAS* 94:39–48

Dormy E, Soward AM, Jones CA, Jault D, Cardin P. 2004. The onset of thermal convection in rotating spherical shells. *J. Fluid Mech.* 501:43–70

Dumberry M, Bloxham J. 2003. Torque balance, Taylor's constraint and torsional oscillations in a numerical model of the geodynamo. *Phys. Earth Planet. Inter.* 140:29–51

Elsasser WM. 1939. On the origin of the Earth's magnetic field. *Phys. Rev.* 55:489–98

Fearn D. 1998. Hydromagnetic flow in planetary cores. *Rep. Prog. Phys.* 61:175–235

Galloway DJ, Proctor MRE, Weiss NO. 1977. Formation of intense magnetic fields near the surface of the Sun. *Nature* 266:686–89

Gillet N, Jones CA. 2006. The quasi-geostrophic model for rapidly rotating spherical convection outside the tangent cylinder. *J. Fluid Mech.* 554:343–69

Gillet N, Jault D, Canet E, Fournier A. 2010. Fast torsional waves and strong magnetic field within the Earth's core. *Nature* 465:74–77

Gillet N, Pais MA, Jault D. 2009. Ensemble inversion of time-dependent core flow models. *Geochem. Geophys. Geosyst.* 10:Q06004

Glatzmaier GA, Coe RS. 2007. Magnetic polarity reversals in the core. See Olson 2007, pp. 283–97

Glatzmaier GA, Coe RS, Hongré L, Roberts PH. 1999. The role of the Earth's mantle in controlling the frequency of geomagnetic reversals. *Nature* 401:885–90

Glatzmaier GA, Roberts PH. 1995. A three-dimensional self-consistent computer simulation of a geomagnetic field reversal. *Nature* 377:203–9

Glatzmaier GA, Roberts PH. 1996a. Rotation and magnetism of the Earth's inner core. *Science* 274:1887–91

Glatzmaier GA, Roberts PH. 1996b. An anelastic evolutionary geodynamo simulation driven by compositional and thermal convection. *Physica D* 97:81–94

Glatzmaier GA, Roberts PH. 1997. Simulating the geodynamo. *Contemp. Phys.* 38:269–88

Grote E, Busse FH. 2000. Hemispherical dynamos generated by convection in rotating spherical shells. *Phys. Rev. E* 62:4457–60

Gubbins D, Jones AL, Finlay CC. 2006. Fall in Earth's magnetic field is erratic. *Science* 312:900–2

Gubbins D, Kelly P. 1993. Persistent patterns in the geomagnetic field during the last 2.5 Myr. *Nature* 365:829–32

Gubbins D, Willis AP, Sreenivasan B. 2007. Correlation of Earth's magnetic field with lower mantle thermal and seismic structure. *Phys. Earth Planet. Inter.* 162:256–60

Hide R. 1974. Jupiter and Saturn. *Proc. R. Soc. Lond. A* 336:63–84

Hoffman KA. 1992. Dipolar reversal states of the geomagnetic field and core mantle dynamics. *Nature* 359:789–94

Holme R. 2007. Large-scale flow in the core. See Olson 2007, pp. 107–30

Holme R, Bloxham J. 1996. The magnetic fields of Uranus and Neptune: methods and models. *J. Geophys. Res. Planets* 101:2177–200

Holme R, Olsen N. 2006. Core surface flow modelling from high-resolution secular variation. *Geophys. J. Int.* 166:518–28

Hughes DW. 2007. Nonlinear effects in mean field dynamo theory. In *Mathematical Aspects of Natural Dynamos*, ed. E Dormy, AM Soward, pp. 79–97. Boca Raton, FL: CRC

Hulot G, Lhuillier F, Aubert J. 2010. Earth's dynamo limit of predictability. *Geophys. Res. Lett.* 37:L06305

Ingersoll AP, Pollard D. 1982. Motions in the interiors and atmospheres of Jupiter and Saturn: scale analysis, anelastic equations, barotropic stability criterion. *Icarus* 52:62–80

Jackson A. 2003. Intense equatorial flux spots on the surface of the Earth's core. *Nature* 424:760–63

Jackson A, Livermore P. 2009. On Ohmic heating in the Earth's core I: nutation constraints. *Geophys. J. Int.* 177:367–82

Jones CA. 2000. Convection driven geodynamo models. *Philos. Trans. R. Soc. Lond. A* 358:873–97

Jones CA. 2003. Dynamos in planets. In *Stellar Astrophysical Fluid Dynamics*, ed. MJ Thompson, J Christensen-Dalsgaard, pp. 159–76. Cambridge, UK: Cambridge Univ. Press

Jones CA. 2007a. Planetary dynamos. In *Mathematical Aspects of Natural Dynamos*, ed. E Dormy, AM Soward, pp. 257–80. Boca Raton, FL: CRC

Jones CA. 2007b. Thermal and compositional convection in the outer core. See Olson 2007, pp. 131–85

Jones CA, Kuzanyan KM. 2009. Compressible convection in the deep atmospheres of giant planets. *Icarus* 204:227–38

Jones CA, Kuzanyan KM, Mitchell RH. 2009. Linear theory of compressible convection in rapidly rotating spherical shells, using the anelastic approximation. *J. Fluid Mech.* 634:291–319

Jones CA, Longbottom AW, Hollerbach R. 1995. A self-consistent convection driven geodynamo model, using a mean field approximation. *Phys. Earth Planet. Inter.* 92:119–41

Jones CA, Soward AM, Mussa AI. 2000. The onset of convection in a rapidly rotating sphere. *J. Fluid Mech.* 405:157–79

Kageyama A, Miyagoshi T, Sato T. 2008. Formation of current coils in geodynamo simulations. *Nature* 454:1106–9

Kageyama A, Sato T. 1997. Velocity and magnetic field structures in a magnetohydrodynamic dynamo. *Phys. Plasmas* 4:1569–75

Kageyama A, Sato T, Watanabe K, Horiuchi R, Hayashi T, et al. 1995. Computer simulation of a magnetohydrodynamic dynamo. II. *Phys. Plasmas* 2:1421–31

Kivelson MG, Khurana KK, Russell CT, Walker RJ, Warnecke J, et al. 1996. Discovery of Ganymede's magnetic field by the Galileo spacecraft. *Nature* 384:537–41

Kono M, Roberts PH. 2002. Recent geodynamo simulations and observations of the geomagnetic field. *Rev. Geophys.* 40:1013

Kono M, ed. 2007. *Treatise on Geophysics*, Vol. 5. Amsterdam: Elsevier

Kuang W, Bloxham J. 1997. An Earth-like numerical dynamo model. *Nature* 389:371–74

Kuang W, Jiang W, Wang T. 2008. Sudden termination of Martian dynamo? Implications from subcritical dynamo simulations. *Geophys. Res. Lett.* 35:L14204

Kuang WJ, Tangborn A, Wei ZG, Sabaka T. 2009. Constraining a numerical geodynamo model with 100 years of surface observations. *Geophys. J. Int.* 179:1458–68

Kutzner C, Christensen UR. 2002. From stable dipolar towards reversing numerical dynamos. *Phys. Earth Planet. Inter.* 131:29–45

Kutzner C, Christensen UR. 2004. Simulated geomagnetic reversals and preferred virtual geomagnetic pole paths. *Geophys. J. Int.* 157:1105–18

Labrosse S, Poirier JP, LeMouel JL. 2001. The age of the inner core. *Earth Planet. Sci. Lett.* 190:111–23

Larmor J. 1919. How could a rotating body such as the Sun become a magnet? *Rep. Br. Assoc. Adv. Sci.* 87:159–60

Lillis RJ, Frey HV, Manga M, Mitchell DL, Lin RP, et al. 2008. An improved crustal magnetic map of Mars from electron reflectometry: highland volcano magmatic history and the end of the martian dynamo. *Icarus* 194:575–96

Malkus WVR. 1994. Energy sources for planetary dynamos. In *Lectures on Solar and Planetary Dynamos*, ed. MRE Proctor, AD Gilbert, pp. 161–79. Cambridge, UK: Cambridge Univ. Press

Maus S, Macmillan S, Lowes F, Bondar T. 2005. Evaluation of candidate geomagnetic field models for the 10th generation of IGRF. *Earth Planets Space* 57:1173–81

Merrill RT, McElhinny MW, McFadden PL. 1996. *The Magnetic Field of the Earth*. Vol. 63 Int. Geophys. Ser. New York: Academic

Miyagoshi T, Kageyama A, Sato T. 2010. Zonal flow formation in the Earth's core. *Nature* 463:793–97

Moffatt HK. 1978. *Magnetic Field Generation in Electrically Conducting Fluids*. Cambridge, UK: Cambridge Univ. Press. 343 pp.

Nellis WJ. 2000. Metallization of fluid hydrogen at 140 GPa (1.4 Mbar): implications for Jupiter. *Planet. Space Sci.* 48:671–77

Olson P, ed. 2007. *Treatise on Geophysics*, Vol. 8. Amsterdam: Elsevier

Olson P, Aurnou J. 1999. A polar vortex in the Earth's core. *Nature* 402:170–73

Olson P, Christensen UR. 2006. Dipole moment scaling for convection-driven planetary dynamos. *Earth Planet. Sci. Lett.* 250:561–71

Olson P, Christensen UR, Glatzmaier GA. 1999. Numerical modeling of the geodynamo: mechanisms of field generation and equilibration. *J. Geophys. Res.* 104:10383–404

Roberts PH. 1968. On the thermal instability of a rotating fluid sphere containing heat sources. *Philos. Trans. R. Soc. Lond. A* 263:93–117

Roberts PH, Jones CA, Calderwood A. 2003. Energy fluxes and ohmic dissipation. In *Earth's Core and Lower Mantle*, ed. CA Jones, AM Soward, K Zhang, pp. 100–29. Philadelphia: Taylor & Francis

Roberts PH, Scott S. 1965. On analysis of the secular variation. 1: A hydromagnetic constraint: theory. *J. Geomagn. Geoelect.* 17:137–51

Rotvig J, Jones CA. 2002. Rotating convection-driven dynamos at low Ekman number. *Phys. Rev. E* 66:056308

Russell CT, Yu ZJ, Kivelson MG. 2001. The rotation period of Jupiter. *Geophys. Res. Lett.* 28:1911–12

Sakuraba A, Roberts PH. 2009. Generation of a strong magnetic field using uniform heat flux at the surface of the core. *Nat. Geosci.* 2:802–5

Sarson GR, Jones CA. 1999. A convection driven geodynamo reversal model. *Phys. Earth Planet. Inter.* 111:3–20

Sarson GR, Jones CA, Zhang K, Schubert G. 1997. Magnetoconvection dynamos and the magnetic fields of Io and Ganymede. *Science* 276:1106–8

Showman AP, Stevenson DJ, Malhotra R. 1997. Coupled orbital and thermal evolution of Ganymede. *Icarus* 129:367–83

Simitev RD, Busse FH. 2005. Prandtl-number dependence of convection-driven dynamos in rotating spherical fluid shells. *J. Fluid Mech.* 532:365–88

Simitev RD, Busse FH. 2008. Toroidal flux oscillation as possible cause of geomagnetic excursions and reversals. *Phys. Earth Planet. Inter.* 168:237–43

Simitev RD, Busse FH. 2009. Bistability and hysteresis of dipolar dynamos generated by turbulent convection in rotating spherical shells. *Europhys. Lett.* 85:19001

Sreenivasan B, Jones CA. 2005. Structure and dynamics of the polar vortex in the Earth's core. *Geophys. Res. Lett.* 32:L20301

Sreenivasan B, Jones CA. 2006a. The role of inertia in the evolution of spherical dynamos. *Geophys. J. Int.* 164:467–76

Sreenivasan B, Jones CA. 2006b. Azimuthal winds, convection and dynamo action in the polar region of the planetary cores. *Geophys. Astrophys. Fluid Dyn.* 100:319–39

Stanley S, Bloxham J. 2006. Numerical dynamo models of Uranus' and Neptune's magnetic fields. *Icarus* 184:556–72

Stanley S, Bloxham J, Hutchison WE, Zuber MT. 2005. Thin shell dynamo models consistent with Mercury's weak observed magnetic field. *Earth Planet. Sci. Lett.* 234:27–38

Stanley S, Elkins-Tanton L, Zuber MT, Parmentier EM. 2008. Mars' paleomagnetic field as the result of a single-hemisphere dynamo. *Science* 321:1822–25

Starchenko S, Jones CA. 2002. Typical velocities and magnetic field strengths in planetary interiors. *Icarus* 157:426–35

Stevenson DJ. 1982. Reducing the non-axisymmetry of a planetary dynamo and an application to Saturn. *Geophys. Astrophys. Fluid Dyn.* 21:113–27

Stevenson DJ. 2003. Planetary magnetic fields. *Earth Planet. Sci. Lett.* 208:1–11
Stevenson DJ. 2007. Nondynamo theories. In *Encyclopaedia of Geomagnetism and Paleomagnetism*, ed. D Gubbins, E Herrero-Bervera, pp. 704–6. New York: Springer
Takahashi F, Matsushima M, Honkura Y. 2005. Simulations of a quasi-Taylor state geomagnetic field including polarity reversals on the Earth Simulator. *Science* 309:459–61
Taylor JB. 1963. The magneto-hydrodynamics of a rotating fluid and the Earth's dynamo problem. *Proc. R. Soc. Lond. A* 274:274–83
Tilgner A. 2007a. Kinematic dynamos with precession driven flow in a sphere. *Geophys. Astrophys. Fluid Dyn.* 101:1–9
Tilgner A. 2007b. Rotational dynamics of the core. See Olson 2007, pp. 207–43
Uno H, Johnson CL, Anderson BJ, Korth H, Solomon SC. 2009. Modeling Mercury's internal magnetic field with smooth inversions. *Earth Planet. Sci. Lett.* 285:328–39
Valet J-P, Meynardier L, Guyodo Y. 2005. Geomagnetic dipole strength and reversal rate over the past two million years. *Nature* 435:802–5
Weiss BP, Berdahl JS, Elkins-Tanton L, Stanley S, Lima EA. 2008. Magnetism on the angrite parent body and the early differentiation of planetesimals. *Science* 322:713–16
Willis AP, Sreenivasan B, Gubbins D. 2007. Thermal core-mantle interaction: exploring regimes for 'locked' dynamo action. *Phys. Earth Planet. Inter.* 165:83–92
Yoder CF, Konopliv AS, Yuan DN, Standish EM, Folkner WM. 2003. Fluid core size of Mars from detection of the solar tide. *Science* 300:299–303
Zatman S, Bloxham J. 1997. Torsional oscillations and the magnetic field within the Earth's core. *Nature* 388:760–63
Zeldovich YB. 1957. The magnetic field in the two-dimensional motion of a conducting turbulent fluid. *Sov. Phys. JETP* 4:460–62
Zhang K. 1992. Spiralling columnar convection in rapidly rotating spherical shells. *J. Fluid Mech.* 236:535–56
Zhang K, Busse FH. 1989. Convection driven magnetohydrodynamic dynamos in rotating spherical shells. *Geophys. Astrophys. Fluid Dyn.* 49:97–116

Annual Review of
Fluid Mechanics

Volume 43, 2011

Contents

Indexes

Errata

An online log of corrections to *Annual Review of Fluid Mechanics* articles may be found at http://fluid.annualreviews.org/errata.shtml